Cement and Concrete Composites 123 (2021) 104150

Contents lists available at ScienceDirect

Cement and Concrete Composites

journal homepage: www.elsevier.com/locate/cemconcomp

Numerical method for predicting flow and segregation behaviors of fresh concrete

Zhisong Xu, Zhuguo Li *

Graduate School of Science and Technology for Innovation, Yamaguchi University, Ube, Yamaguchi, Japan

ARTICLE INFO

Keywords:
Fresh concrete
Flow simulation
Static segregation
Dynamic segregation
Double-phase & multi-particle model

ABSTRACT

Current meshless particle methods are able to simulate the flow of fresh concrete, but fail to predict the segregation since fresh concrete is regarded as homogeneous fluid. This study aims to develop a numerical approach to predict the segregation of coarse aggregate (CA) in fresh concrete together with the flow behavior. A double-phase & multi-particle (DPMP) model was proposed to describe fresh concrete, which treats fresh concrete as a double-phase fluid composed of matrix mortar and the CA particles that had random shapes, size distribution, and different density from matrix mortar. Each CA particle was formed by the element particles, of which number was dependent on the size and shape of described CA particle. Three types of inter-particle interaction, including CA-CA particles, CA-mortar particles, and two mortar particles, were investigated, respectively. Then, based on the complete implicit MPS (I-MPS) method and the DPMP model, the L-box flow of two series of high fluidity concrete were simulated. The ability of the proposed numerical approach to simultaneously simulate the flow and segregation behaviors of fresh concrete was confirmed. Moreover, this numerical method can analyze the changes of localized rheological parameters of segregated concrete.

1. Introduction

Concrete has been widely used as a main material to construct building, road, bridge and tunnel, etc. With the advance of sustainable concrete structures, the performance demands for concrete have been rising. Benefiting from the development and usage of chemical and mineral admixtures, especially high-range water reducing agent, the performance of concrete has been improved. As a result, many kinds of high-performance concretes have been developed, such as self-compacting concrete (SCC) [1]. The rheological performance of fresh concrete shows diversity and complexity. For ensuring the quality of concrete construction, fresh concrete should have appropriate workability. Tanigawa [2] proposed the concept and method of numerical flow simulation-based workability evaluation of concrete in 1988. Workability is the ability of fresh concrete to be easily transported and cast into formwork without excessive segregation. Workability can be subdivided into flowability, filling ability, passing ability, pumpability, segregation resistance, etc. Among these, the main concerns are flowability and segregation resistance. The flowability determines the ease of construction, and the segregation resistance affects the quality of hardened concrete, which includes static and dynamic segregation resistance [3]. Static segregation refers to that fresh concrete constituents separate from each other in rest state. Dynamic segregation refers to that fresh concrete segregates during flowing in pumping pipe or formwork or during vibrating. Once the segregation takes place, the aggregate distribution in concrete becomes uneven. The segregation will affect casting efficiency in construction stage, even induce pumping blockage. After hardened, the mechanical property and durability of segregated concrete will get worse [4]. Thus, it is an issue to predict the segregation behavior of fresh concrete during construction.

In order to measure the segregation degree of concrete and evaluate the segregation resistance of fresh concrete, many measurement methods have been proposed [3,5–8]. Using these test methods, the segregation resistance of fresh concretes has been successfully evaluated [5,9–12]. Nevertheless, the current researches on the segregation of fresh concrete are almost experimental approach. Because of the limitation of the measurement methods, it is impossible to observe and analyze the segregation movement of aggregate particles during the flow of fresh concrete. The change in the flowability of fresh concrete once the segregation occurs cannot be evaluated experimentally. Moreover, the experimental need a lot of materials, and the experimental results of segregation have poor repeatability. Although the test

* Corresponding author.
E-mail address: li@yamaguchi-u.ac.jp (Z. Li).

https://doi.org/10.1016/j.cemconcomp.2021.104150
Received 2 February 2021; Received in revised form 11 June 2021; Accepted 19 June 2021
Available online 9 July 2021

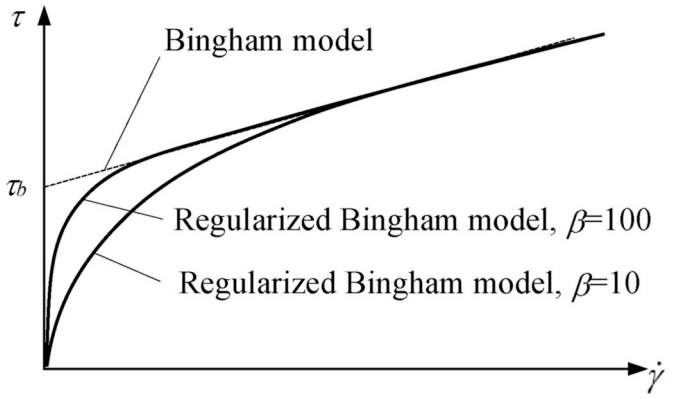

Fig. 1. Original and regularized Bingham models.

methods would qualitatively evaluate the segregation resistance, there is still lack of simple, precise and widely accepted experimental method.

However, numerical flow simulation-based workability evaluation method is an inexpensive and efficient approach. Numerical simulation is also expected to be used to evaluate the segregation resistance besides flowability. In various numerical approaches, it is considered that the meshless particle methods, such as moving particle semi-implicit (MPS) and smooth particle hydrodynamics (SPH), are suitable for large deformation problem with free surface [13]. These meshless particle methods [14–17] have been used to simulate and predict the flow of many fresh concretes, and a complete implicit improved MPS (I-MPS) method [14] was confirmed to be more appropriate for fresh concrete. However, fresh concrete in these simulations is generally regarded as a homogenous fluid, and is represented by round or spheric particles with the same density and dimensions. Therefore, present numerical approaches are unable to describe the heterogeneous feature and to simulate the segregation behavior of fresh concrete. Indeed, meshless particle methods are able to treat with the interactions among fluid particles, thus have the potential to simulate heterogeneous characteristic of concrete and provide information about the static and dynamic segregation of fresh concrete.

In this paper, we tried to develop a numerical flow approach of fresh concrete based on the I-MPS method, which can predict the segregation behavior together with the flow behavior of fresh concrete simultaneously. A Double-Phase & Multi-Particle (DPMP) model was proposed to express fresh concrete in the numerical simulation. In the DPMP model, fresh concrete is composed of matrix mortar and coarse aggregate (CA). These two phases have different densities and rheological parameters. Each CA particle is represented by several round or spherical elementary particles which have the same size with the matrix mortar particles. The interactions between mortar-mortar particles, CA-CA particles, and mortar-CA particles were discussed and addressed, respectively. This numerical flow approach was verified by simulating the L-box flow of high fluidity concrete. Both the static segregation and dynamic segregation behaviors were investigated quantitatively. Moreover, the numerical results can clarify the changes in the localized rheological parameters of fresh concrete after segregation.

2. Numerical simulation method

2.1. Rheological model of fresh concrete

The rheological behavior of fresh concrete is approximately described by Bingham model. When shear stress is greater than the yield stress of fresh concrete, shear flow is observed. The constitutive equation is written as:

$$\tau = \tau_b + \mu_b \cdot \dot{\gamma} \tag{1}$$

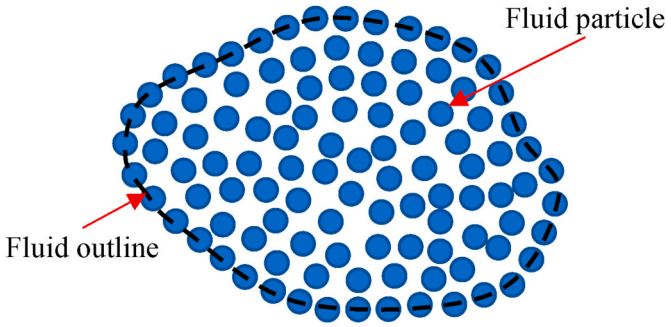

Fig. 2. Imaged fluid particles of I-MPS.

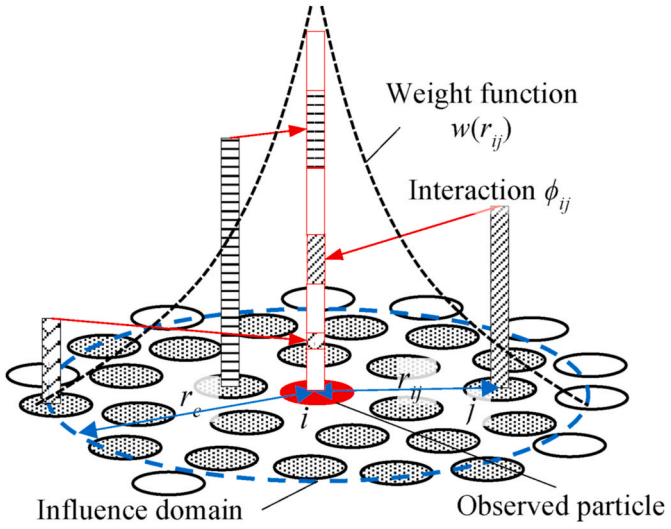

Fig. 3. Interaction between particle i and neighbor particles.

where, τ is shear stress, τ_b is yield stress, μ_b is plastic viscosity, $\dot{\gamma}$ is shear strain rate.

The dynamic viscosity μ of fresh concrete, defined as a ratio of shear stress to shear strain rate, is used in the numerical simulation. As the shear stress is equal to the yield stress, the shear rate becomes to zero, which makes the dynamic viscosity diverge. Thus, it is difficult to apply the Bingham model directly in numerical simulation because of the discontinuity in the constitutive law. To overcome this problem, the dynamic viscosity is calculated by the regularized Bingham model [18] as shown in Eq. (2). Both the original and regularized Bingham model are shown in Fig. 1. Although the two Bingham models are the same at high shear rate, the larger the β in Eq. (2), the sharper the $\tau - \dot{\gamma}$ curve in small shear rate range, and the closer the regularized Bingham model is to the original Bingham model. It is reported that the solution is insensitive to β when $\beta > 10$ [19]. In this study, the β was set to be 100.

$$\mu = \mu_b + \tau_b \frac{1 - e^{-\beta\dot{\gamma}}}{\dot{\gamma}} \tag{2}$$

where, β is a regularization parameter related to the transition between solid and fluid regimes.

2.2. Boundary conditions

The no-slip boundary condition was adopted, i.e., the particle velocity along the flow boundary was zero or assigned to be its moving velocity. The Dirichlet boundary condition [20] was adopted to solve the pressure Poisson equation. The pressure on the free surface was set to be zero.

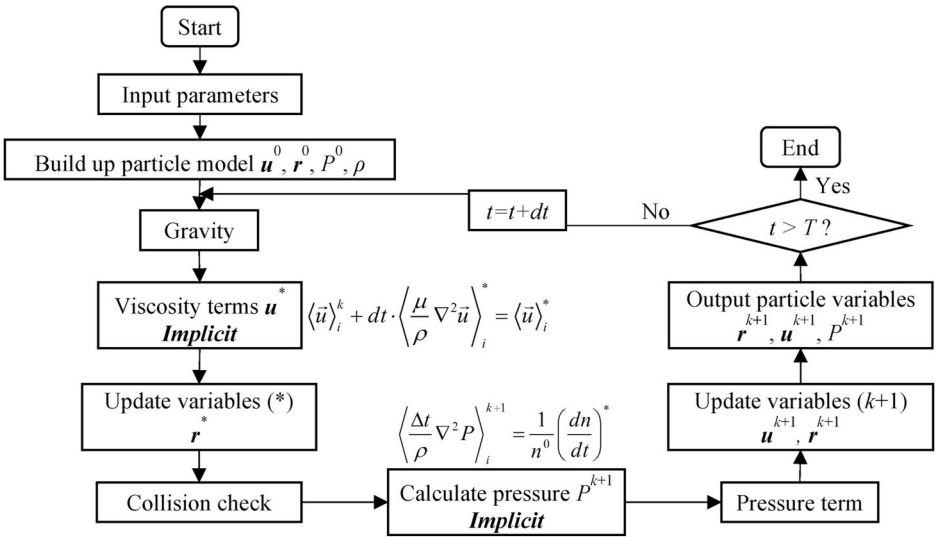

Fig. 4. Flowchart of I-MPS algorithm.

2.3. Algorithm of I-MPS method

In this study, a complete implicit improved MPS (I-MPS) method is used. I-MPS treats fluid as incompressible not like traditional Smoothed Particle Hydrodynamics (SPH), and I-MPS is more efficient than semi-implicit method MPS because the viscosity term is also solved by implicit algorithm, and the higher order Laplacian model is used, resulting in more stable computational results [14]. As a meshless particle method, in the I-MPS, fluid is described by imaginary particles, as shown in Fig. 2. These particles are just mathematical points, but for expressing the physical characteristics of the fluid, the physical properties, such as size, density, position, velocity, viscosity, and pressure, are given to these imaginary particles. The force applied to the observed particle is obtained by a weighted average of the interaction with other particles in the influence domain (as shown in Fig. 3). In the I-MPS, the particles are assumed to be incompressible, and particle density is a constant. To instead of the particle density, the particle number density n is used, which is the integral summation of the weight function in the influence domain. The weight function (kernel) is employed in the I-MPS, as shown in Eq. (3).

$$w(r_{ij}) = \begin{cases} \dfrac{r_e}{r_{ij}} - 1, & 0 < r_{ij} < r_e \\ 0, & r_{ij} \geq r_e \end{cases}, r_{ij} = \left| \vec{r}_j - \vec{r}_i \right| \tag{3}$$

where, r_{ij} is distance between two particles, and r_e is radius of influence domain.

The governing equations used in the numerical flow simulation are written as:

$$\begin{cases} \nabla \cdot \vec{u} = 0 \\ \dfrac{d\vec{u}}{dt} = \vec{g} + \dfrac{\mu}{\rho} \nabla^2 \vec{u} - \dfrac{1}{\rho} \nabla P \end{cases} \tag{4}$$

where, ρ is density of fluid, $\vec{u}$ is velocity, t is time, P is pressure, $\vec{g}$ is gravitational acceleration, and μ is dynamic viscosity of fluid.

The flowchart of the I-MPS algorithm is shown in Fig. 4. The details can be found in Ref. [14]. The Laplacian in the velocity Poisson equation for calculating the viscous terms (the second term of right side of the motion equation shown in Eq. (4)) is discretized by higher order Laplacian (HL) scheme [21] as:

$$\left\langle \frac{\mu}{\rho} \nabla^2 \vec{u} \right\rangle_i = \frac{5-d}{n^0} \frac{\mu}{\rho} \sum_{i \neq j} \frac{\vec{u}_{ij} r_e}{r_{ij}^3} \tag{5}$$

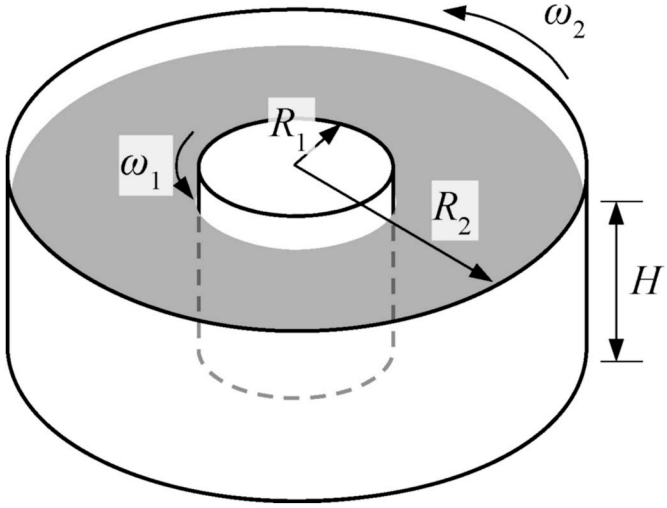

Fig. 5. Taylor-Couette flow model.

where, d is model dimension, and equals to 3 in three-dimensions. n^0 is a constant representing the initial particle number density.

The Laplacian in the pressure Poisson equation for calculating the inter-pressure of fluid particles is discretized as:

$$\left\langle \frac{1}{\rho} \nabla^2 P \right\rangle_i^{k+1} = \frac{5-d}{n^0} \frac{1}{\rho} \sum_{j \neq i} \left(P_j^{k+1} - P_i^{k+1} \right) \frac{r_e}{\left| \vec{r}_j^* - \vec{r}_i^* \right|^3} \tag{6}$$

For stabilizing the numerical calculation, the pressure gradient in the I-MPS is expressed by the following discrete equation:

$$\langle \nabla P \rangle_i^{k+1} = \frac{d}{n^0} \sum_{j \neq i} \left[\frac{P_j^{k+1} - P_{i,min}^{k+1}}{\left| \vec{r}_j^* - \vec{r}_i^* \right|^2} \left(\vec{r}_j^* - \vec{r}_i^* \right) \left(r_{ij}^* \right) \right] \tag{7}$$

where, $P_{i,min}$ is the minimum pressure among the neighboring particles.

2.4. Validation of I-MPS method

2.4.1. Theoretical solution of Taylor-Couette flow

In order to verify again the reliability of the I-MPS method for the

Table 1
Parameters for Taylor-Couette flow.

Radius R_1 (m)	0.05	Height H (m)	0.10
Angular velocity ω_1 (rad/s)	1.00	Density ρ (kg/m^3)	2300.00
Radius R_2 (m)	0.15	Yield stress τ_b (Pa)	0.00
Angular velocity ω_2 (rad/s)	0.00	Plastic viscosity μ_b (Pa·s)	100.00

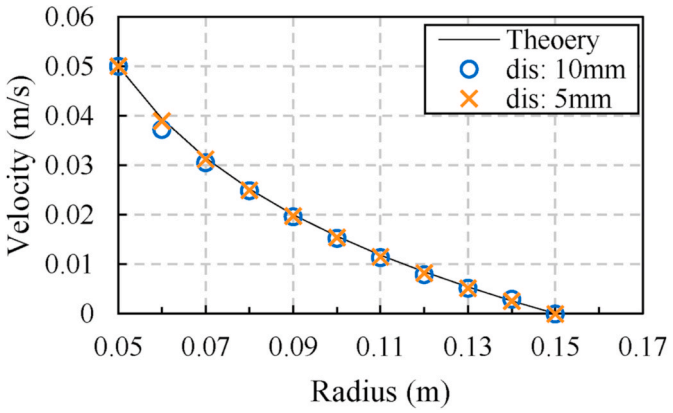

Fig. 6. Rotation velocity profiles in Taylor-Couette flow.

flow analysis of fresh concrete, and to discuss the reasonable particle size for the flow simulation, the Taylor-Couette flow was first simulated in this study. The Taylor-Couette flow model is shown in Fig. 5. The fluid is located between two cylinders. The inner cylinder has a radius of R_1, and rotates at an angular speed of ω_1. The outer cylinder has a radius of R_2, and rotates at an angular speed of ω_2. Assuming there is no slip between the fluid and the walls of cylinders, the fluid is sheared between the two cylinders, and occurs a steady flow. The fluid only flows in the circumferential direction. Thus, the continuity equation and motion equation of the fluid can be simplified as:

$$\begin{cases} \dfrac{\partial u_R}{\partial \theta} = 0, & \dfrac{\mu}{\rho}\dfrac{\partial}{\partial R}\left[\dfrac{1}{R}\dfrac{\partial}{\partial R}(Ru_R)\right] = 0 \\ \dfrac{u_R^2}{R} = \dfrac{1}{\rho}\dfrac{\partial P}{\partial R}, & g - \dfrac{1}{\rho}\dfrac{\partial P}{\partial z} = 0 \end{cases} \tag{8}$$

where, u_R is circumferential flow velocity at the radius of R.

For fresh concrete, since the yield stress is usually not zero, its dynamic viscosity changes with the shear rate, as seen in Eq. (2). Thus, in order to simplify the calculation of Taylor-Couette flow, the yield stress of fresh concrete was set to zero here, the dynamic viscosity became a constant. Based on Eq. (8), the circumferential flow velocity u_R of fresh concrete at the radius of R can be obtained, as shown in the follow:

$$u_R = \frac{\omega_2 R_2^2 - \omega_1 R_1^2}{R_2^2 - R_1^2} R + \frac{(\omega_1 - \omega_2) R_1^2 R_2^2}{R_2^2 - R_1^2} \frac{1}{R} \tag{9}$$

The diameter and property parameters for Taylor-Couette flow test are listed in Table 1. Substituting the parameters in Table 1 into Eq. (9), the circumferential flow velocity profile along the radius is calculated, the theoretical result of Taylor-Couette flow is shown in Fig. 6.

2.4.2. I-MPS simulation

The Taylor-Couette flow simulations were done by using different particle sizes (*dis*), which were 10 mm and 5 mm, respectively, for determining suitable size of fluid particle used in the simulation of I-MPS. The simulated flow velocities are shown and compared to the theoretical results in Fig. 6. When the particle diameter was 10 mm, the simulated results were almost consistent with the theoretical results, but there was small error in the area near the walls of cylinders. When the particle diameter was 5 mm, the simulated velocity profile in the entire flow profile was consistent with the theoretical result. Therefore, the I-MPS method is able to simulate the flow of fresh concrete provided that the appropriate particle size is used. The particle diameter in the following simulation was set as 5 mm.

3. Numerical analysis model of fresh concrete

In the I-MPS simulation [14], if treating fresh concrete as a fluid consisting of spherical particles of the same size and density according to the traditional MPS, it is impossible to simulate the behavior of coarse aggregate in fresh concrete. In order to simulate the segregation of CA, in this study we improved the I-MPS method by treating fresh concrete as double-phase granular fluid, and considering the difference in size and shape between CA particles and the difference in density between CA and mortar.

3.1. Constituent model of fresh concrete

Fresh concrete can be regarded as particle assembly with water, binder, and aggregate particles ranging from a few microns to tens centimeters in size. However, fresh concrete is usually modeled as single-phase homogeneous granular material in many numerical simulations of particle methods [15,17,22]. To track the segregation behavior of coarse aggregate, and to analyze the effect of coarse aggregate's segregation on the flow behavior of fresh concrete, it is necessary to treat the coarse aggregate as a separate component of fresh concrete. That is, fresh concrete should be considered as a discontinuous double-phase system composed of matrix mortar and coarse aggregate particles. As shown in Fig. 7, volume V of fresh concrete is a sum of

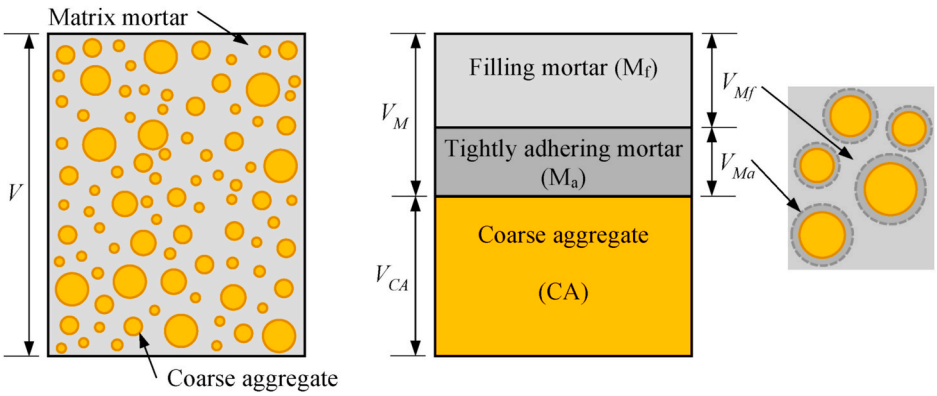

Fig. 7. Constituent model of fresh concrete.

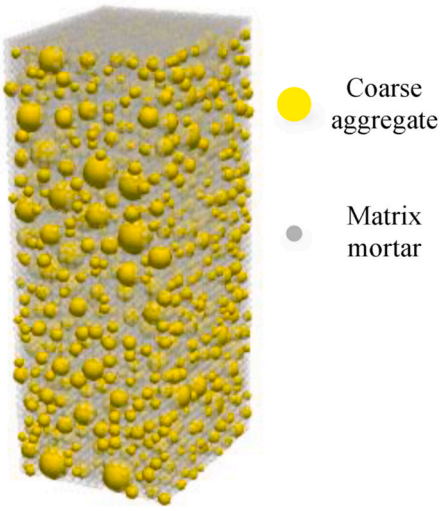

Fig. 8. Constituent model of fresh concrete.

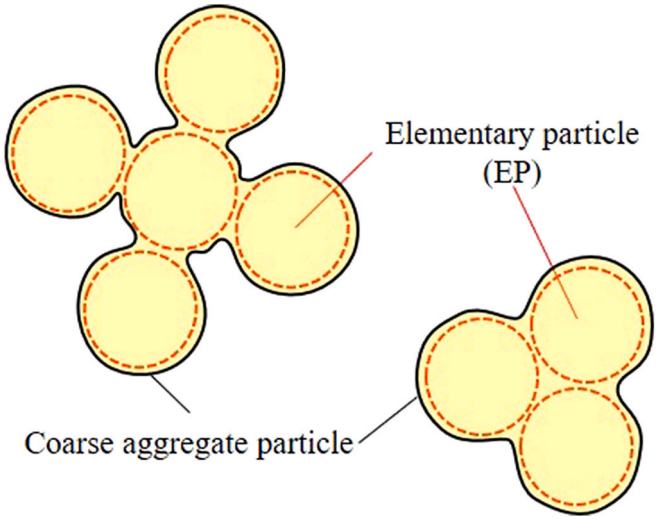

Fig. 9. Formation of coarse aggregate particle.

matrix mortar's volume V_M and coarse aggregate's volume V_{CA}. Based on the excess paste theory [23,24], the matrix mortar is divided into: the filling mortar (*Mf*) and the mortar tightly adhering to coarse aggregate (*Ma*). The filling mortar fills in the voids and gaps between coarse aggregates, while the tightly adhering mortar covers the surface of coarse aggregate particles. The corresponding volumes are represented by V_{Mf} and V_{Ma}, respectively.

In the simulation, fresh concrete was represented by matrix mortar particles and CA particles. The double-phase & multi-particle (DPMP) model was used as the constituent model to describe fresh concrete for numerical flow simulation, as shown in Fig. 8. CA particles have different sizes and random shapes, but matrix mortar phase is represented by spherical particles with same diameter. CA particle is formed by several elementary particles, of which the number is dependent on the geometry and dimension of formed CA particle, as shown in Fig. 9. The shape of the CA particles is expressed by the outer contour of the elementary particles. The elementary particle is spherical and has the same size as the mortar particle but its specific gravity is different from the mortar particle. Fig. 10 shows examples of formed CA particles with different sizes and shapes. The CA particles used in the numerical calculation have random shapes, but in the simulation output, for easy visualization of simulation results, the CA particles are expressed as spheres in 3D simulation or circles in 2D simulation as shown in Fig. 7, and in Fig. 12 and Fig. 13 mentioned later. The more the element particles used for forming a CA particle, i.e., reducing the size of element particle but increasing the its number, the closer the shape of the formed particle is to its actual shape. However, using smaller and more element particles to form CA particles will certainly increase calculation time. Therefore, the size setting of elementary particle needs to be balanced between the calculation time and the accuracy of CA shape representation.

3.2. Interaction models between various particles in fresh concrete

To calculate the movement of the particles, it is necessary to figure out the interactions between the particles. In this study the fresh concrete was considered as a double-phases fluid rather than a homogeneous fluid, composed of matrix mortar particles and CA particles. Thus, the following three kinds of interaction between particles should be clarified in advance.

3.2.1. Between mortar particles

The Bingham constants of the matrix mortar can be measured directly by a rheometer, then, the dynamic viscosity of mortar particle is calculated by Eq. (2). For the accuracy of numerical simulation, the harmonic mean interparticle viscosity is recommended by Shakibaeinia et al. [25]. The viscosities interaction between mortar particles can be calculated by the following multi-viscosity model:

$$\left\langle \frac{\mu}{\rho}\nabla^2\vec{u}\right\rangle_{ij} = \frac{5-d}{n^0}\cdot\frac{2\mu_i\mu_j}{\mu_i+\mu_j}\cdot\frac{1}{\rho_M}\cdot\frac{\vec{u}_{ij}r_e}{r_{ij}^3} \tag{10}$$

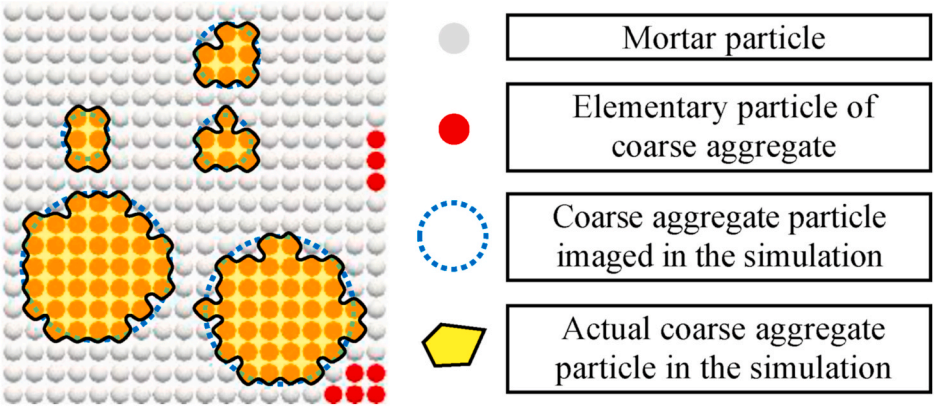

Fig. 10. Random size and shape of coarse aggregate particles (2D).

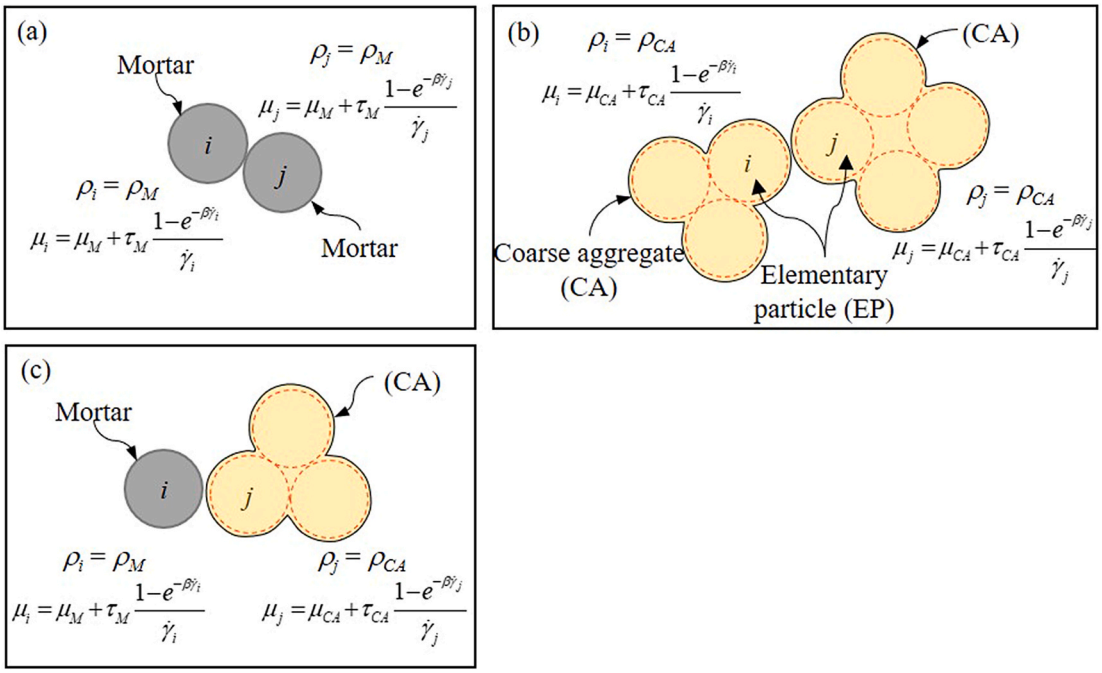

Fig. 11. Three types of particle interaction models in fresh concrete.

where, ρ_M is density of matrix mortar.

The Laplacian in the pressure Poisson equation for calculating the inter-pressure of mortar particles is modified as:

$$\left\langle \frac{1}{\rho}\nabla^2 P \right\rangle_{ij}^{k+1} = \frac{5-d}{n^0}\cdot\frac{1}{\rho_M}\cdot\left(P_j^{k+1} - P_i^{k+1}\right)\cdot\frac{r_e}{\left|\vec{r}_j^{\,*} - \vec{r}_i^{\,*}\right|^3} \tag{11}$$

3.2.2. Between CA particles

CA particles are regarded as rigid materials, and the interaction between them should be friction theoretically. However, in order to use the same constitutive model to calculate the particle movement, the Bingham model was used to describe the displacement resistance of CA particles in this study. In addition, the CA particles are wrapped in a thin mortar layer as described in Fig. 7, so that it is somehow reasonable that the shear resistance of CA particles follows the Bingham model.

Due to the assumption that the CA particle is formed by several elementary particles, the interaction between two CA particles can be expressed by the interactions between the elementary particles. The interaction between two elementary particles is calculated by the same method as the interaction between mortar particles, as shown in Eqs. (12) and (13).

$$\left\langle \frac{\mu}{\rho}\nabla^2 \vec{u} \right\rangle_{ij} = \frac{5-d}{n^0}\cdot\frac{2\mu_i\mu_j}{\mu_i+\mu_j}\cdot\frac{1}{\rho_{CA}}\cdot\frac{\vec{u}_{ij}r_e}{r_{ij}^3} \tag{12}$$

$$\left\langle \frac{1}{\rho}\nabla^2 P \right\rangle_{ij}^{k+1} = \frac{5-d}{n^0}\cdot\frac{1}{\rho_{CA}}\cdot\left(P_j^{k+1} - P_i^{k+1}\right)\cdot\frac{r_e}{\left|\vec{r}_j^{\,*} - \vec{r}_i^{\,*}\right|^3} \tag{13}$$

where, ρ_{CA} is density of coarse aggregate.

3.2.3. Between mortar particle and CA particle

The interaction between mortar particle and coarse aggregate particle is more complicated than the above two cases, because two kinds of particles have different rheological properties and densities. Duan et al. [26] suggested to use arithmetic mean density to improve the stability of the numerical results. The viscous interaction can be calculated by Eq. (14).

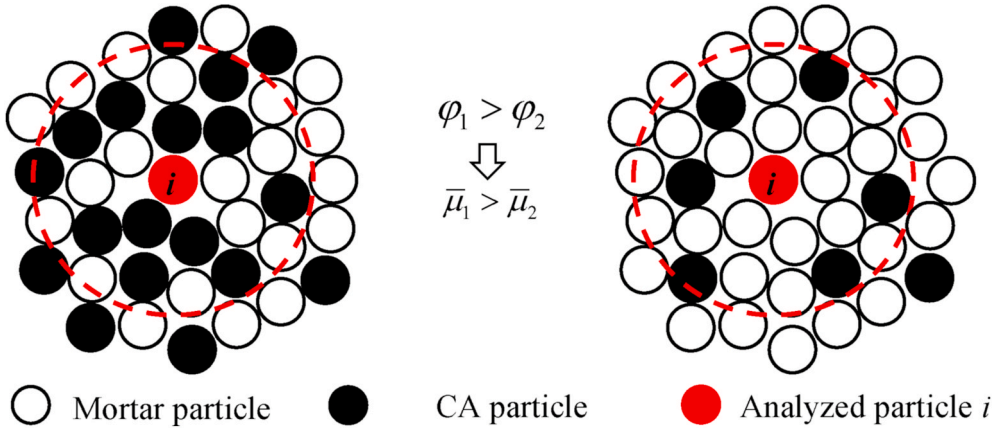

Fig. 12. Change of mean dynamic viscosity with CA volume fraction (left: φ_1, right: φ_2).

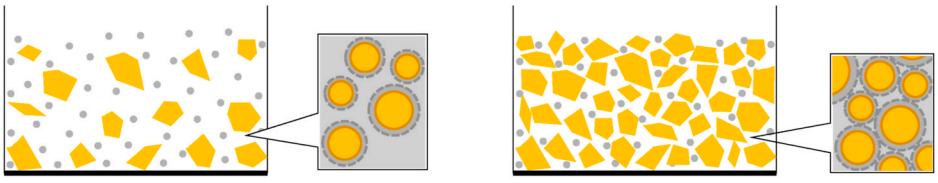

Fig. 13. Schematic diagram of normal fresh concrete and CA particle system.

$$\left\langle \frac{\mu}{\rho}\nabla^2\vec{u}\right\rangle_{ij} = \frac{5-d}{n^0}\cdot\frac{2\mu_i\mu_j}{\mu_i+\mu_j}\cdot\frac{2}{\rho_i+\rho_j}\cdot\frac{\vec{u}_{ij}r_e}{r_{ij}^3} \tag{14}$$

The Laplacian in the pressure Poisson equation is modified by the following multi-density model:

$$\left\langle \frac{1}{\rho}\nabla^2 P\right\rangle_{ij}^{k+1} = \frac{5-d}{n^0}\cdot\frac{2}{\rho_i+\rho_j}\cdot\left(P_j^{k+1}-P_i^{k+1}\right)\cdot\frac{r_e}{\left|\vec{r}_j^{\,*}-\vec{r}_i^{\,*}\right|^3} \tag{15}$$

Three types of interaction models of particles are summarized in Fig. 11. The pressure gradient shown in Eq. (7) is divided into two terms for fresh concrete composed of two kinds of particles with different densities as follows [26]:

$$\begin{aligned}\left\langle \frac{1}{\rho}\nabla P\right\rangle_i &= \frac{d}{n^0}\sum_{j\neq i}\left[\frac{2\left(P_j-P_i\right)}{\left(\rho_i+\rho_j\right)\left|\vec{r}_j^{\,*}-\vec{r}_i^{\,*}\right|^2}\left(\vec{r}_j^{\,*}-\vec{r}_i^{\,*}\right)w\left(r_{ij}^*\right)\right]\\ &+\frac{d}{n^0}\sum_{j\neq i}\left[\frac{\left(P_i-P'_{i,\mathrm{inn}}\right)}{\rho_i\left|\vec{r}_j^{\,*}-\vec{r}_i^{\,*}\right|^2}\left(\vec{r}_j^{\,*}-\vec{r}_i^{\,*}\right)w\left(r_{ij}^*\right)\right]\end{aligned} \tag{16}$$

where, $P'_{i,min}$ is the minimum pressure among the same type of neighboring particles of particle i.

The harmonic mean dynamic viscosity $\vec{\mu}_i$of particle i can be calculated by:

$$\overline{\mu}_i = \frac{N_i}{\sum_{j\neq i}^{N_i}\frac{1}{\mu_j}} \tag{17}$$

where, N_i is number of neighboring particles in the influence domain of particle i.

As shown in Fig. 12, the larger the volume fraction (φ) of CA, the larger the probability of CA particles existing in an influence domain of particle i, and the higher the mean dynamic viscosity ($\overline{\mu}$) of particle i. Thus, Eq. (17) can reflect the effect of CA's volume fraction on the dynamic viscosity of fresh concrete, i.e., fresh concrete with larger volume fraction of CA has higher dynamic viscosity. Moreover, if fresh concrete segregates, the CA distribution becomes uneven, part of concrete has a larger CA volume fraction, it presents a higher dynamic viscosity. Therefore, the DPMP model has the potential to reflect the influence of CA segregation.

3.3. Rheological parameters for expressing particle displacement resistance

When considering the interaction between particles follows the Bingham model, the Bingham constants describing three types of particle interaction, shown in Fig. 11, should be determined first. The Bingham constants (μ_M, τ_M) of matrix mortar can be measured directly by a rheometer, as mentioned above. However, there is currently no method to determine the Bingham constants (μ_{CA}, τ_{CA}) of CA particle system. As shown in Fig. 13 (b), the volume fraction of CA in the CA particle system is larger than that in normal fresh concrete, the CA particles are in close contact by tightly adhering mortar, and the filling mortar is just used to fill the voids between CA particles.

Fig. 14. Coarse aggregates with different sizes and shapes.

Ferraris and deLarrard [27,28] found that either the plastic viscosity or yield stress of fresh concrete is a function of the volume fraction of solid material and the maximum packing volume fraction of the individual components. Based on the Einstein's model [29], Roscoe [30] and Krieger-Dougherty [31] further proposed the models to predict the plastic viscosity of suspension by the volume fraction of dispersed spherical particles and their maximum packing volume fraction. Struble and Sun [32] modified the model and suggested an equation to predict the plastic viscosity of fresh concrete, as shown in the following:

$$\mu = \mu_M\cdot\left(1-\frac{\varphi}{\varphi_m}\right)^{-\mu_*\cdot\varphi_m} \tag{18}$$

where, μ_M is viscosity of matrix mortar, φ is volume fraction of coarse aggregate, φ_m is maximum packing volume fraction of coarse aggregate, μ_* is intrinsic viscosity of system.

Moreover, Chateau et al. [33], provided a prediction equation of yield stress of fluid as follows:

$$\tau = \tau_M\cdot\sqrt{(1-\varphi)\cdot\left(1-\frac{\varphi}{\varphi_m}\right)^{-\tau_*\cdot\varphi_m}} \tag{19}$$

where, τ_M is yield stress of matrix mortar, τ_* is intrinsic yield stress of system.

Both μ_* and τ_* are 2.5 for the suspension consisting of spherical particles with the same size [32,33]. However, CA particles have irregular shapes and random sizes, as shown in Fig. 14. Therefore, for estimating the Bingham constants (μ_{CA}, τ_{CA}) of the CA particle system, it is necessary to first determine the intrinsic constants μ_* and τ_*. Eqs. (18) and (19) have already been used to successfully estimate the plastic viscosity and yield stress of fresh concrete [34–37]. Hence, by using the measured Bingham constants of matrix mortar and fresh concrete, the μ_* and τ_* and can be estimated on the basis of Eqs. (18) and (19).

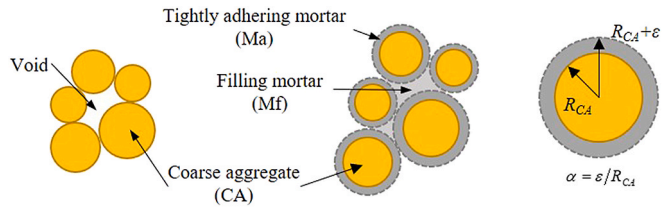

Fig. 15. Increasement of equivalent size of CA particle due to the tightly adhering mortar.

Here, the volume fraction of CA in the CA particle system is donated as φ', and the φ_m of the CA particle system is the maximum packing volume fraction of CA. The calculated Bingham constants by Eqs. (18) and (19) were used as the rheological parameters of CA particle system in the numerical simulation. The following will discuss the volume fraction φ' of CA in the CA particle system.

Originally, the packing volume fraction φ_0 of CA is a ratio of CA volume (V_{CA}) to the sum of CA volume and void volume (V_{Air}) among CA particles, i.e., $V_{CA}/(V_{CA}+V_{Air})$. However, in fresh concrete, CA particle is surrounded by the tightly adhering mortar, as mentioned in Fig. 13, so that the distance between adjacent CA particles is increased. Therefore, the corresponding volume fraction φ' of CA in the CA particle system is less than φ_0. Based on the schematic diagram in Fig. 15, the φ' can be calculated as $V_{CA}/(V_{CA}+V_{Mf}+V_{Ma})$. Assuming all the CA particles are spherical, it is proposed in Ref. [38] that when the packing volume fraction of CA is between 0.52 and 0.74, the thickness of the mortar adhering to CA particle is proportional to the radius (R_{CA}) of the CA particle. In the CA particle system, the packing volume fraction φ_0 of CA equals to the maximum packing volume fraction φ_m, which normally falls in the range of 0.52–0.74. If denoting the ratio of the thickness (ε) of tightly adhering mortar layer to R_{CA} as α, the relationship between α and φ_m (maximum packing volume fraction of CA) can be described as [38]:

$$\alpha = e^{(2.9-10.3\varphi_m)} + 0.077, \varphi_m \in (0.52, 0.74) \tag{20}$$

The φ_m of CA used in this study was 0.592, based on Eq. (20), α was calculated as 0.118. The size distribution of the used CA was 5 mm–20 mm, i.e., the radius of the CA particle was in the range of 2.5 mm–10 mm. The thickness ε of tightly adhering mortar layer was thin and ranged from 0.295 mm to 1.180 mm.

The volume of adhesive mortar layer can be calculated as:

$$V_{Ma} = \frac{4\pi}{3}\sum (R_{CA}+\varepsilon)^3 - \frac{4\pi}{3}\sum R_{CA}^3 = (1+\alpha)^3 V_{CA} - V_{CA} \tag{21}$$

where, R_{CA} is radius of CA particle, ε is thickness of tightly adhering mortar layer.

For the CA particle wrapped by the tightly adhering mortar, its total radius is $(1+\alpha)$ times its original size of CA, thus its total volume becomes $(1+\alpha)^3$ times CA's volume. Correspondingly, the void volume among CA particles will increase at the same times, that is, the volume V_{Mf} of the filling mortar is equal to $(1+\alpha)^3 \cdot V_{Air}$. Thus, the volume fraction φ' of CA in the CA particle system can be calculated as follows:

$$\begin{aligned}\varphi' &= \frac{V_{CA}}{V_{CA}+V_{Mf}+V_{Ma}} = \frac{V_{CA}}{V_{CA}+(1+\alpha)^3 V_{Air}+(1+\alpha)^3 V_{CA}-V_{CA}} \\ &= \frac{1}{(1+\alpha)^3}\frac{V_{CA}}{V_{CA}+V_{Air}} = \frac{\varphi_m}{(1+\alpha)^3}\end{aligned} \tag{22}$$

Once the values of μ_*, τ_*, φ', and φ_m are known, Eqs. (18) and (19) are used to calculate μ_{CA} and τ_{CA}, considering the CA particle system as a suspension. The determining methods of all rheological parameters in numerical simulation are shown in Fig. 16.

3.4. Movement calculation of coarse aggregate particle

The movement of coarse aggregates (CA) is calculated by two steps (see Fig. 17), using the Passively Moving Solid (PMS) model [39]. In the first step, the movements of elementary particles are calculated, which are caused by their self-gravity and the interactions between the elementary particles and between elementary particles and mortar particles. In the second step, the calculated velocities and positions of

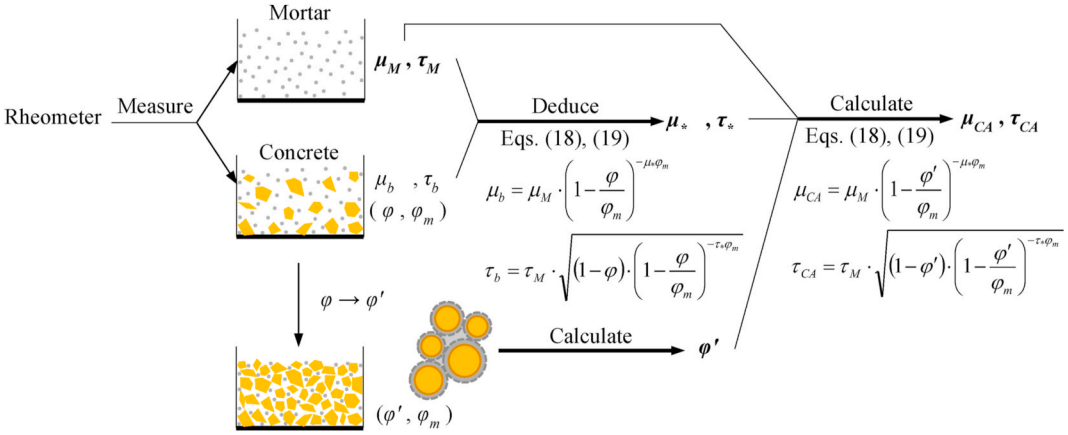

Fig. 16. Determination of rheological parameters for three types of particle interaction.

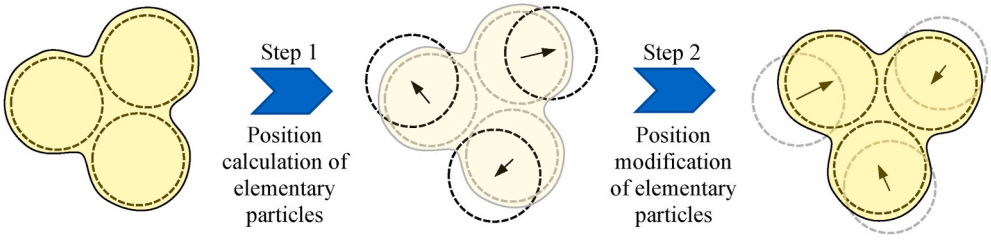

Fig. 17. Position calculation and modification of CA particle.

Table 2
Mix proportions and consistency of high fluidity concretes.

Series	w/b	Unit mass (kg/m^3)						Vol (%)	Bulk density (kg/m^3)	*Sl* (cm)	*Sf* (mm)	t_{500} (s)
		Water	Cement	Fly ash	Sand	Crashed stone	HRWRA					
No.1	0.30	170	283	283	767	830	8.5	31.0	2385	27.0	690	8.5
No.2	0.45	170	189	189	845	911	5.7	34.6	2393	24.5	640	6.0

[Notes:] w/b is water-to-binder ratio by mass, HRWRA is high-range water-reducing agent, Vol is volume fraction of coarse aggregate in concrete, *Sl* is slump value, *Sf* is slump flow value, and t_{500} is flow time of 500 mm.

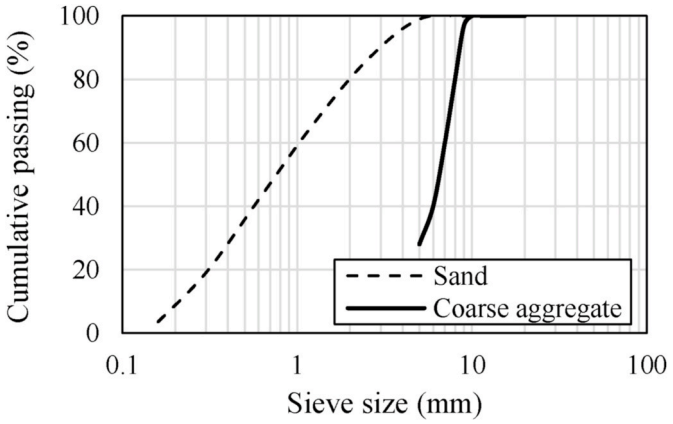

Fig. 18. Particle-size distribution curves of fine aggregate and coarse aggregate used.

elementary particles are revised on basis of the conservation of angular momentum to ensure that the shape of the CA particle is unchanged. The angular momentum of the CA particle in time-step k+1 is calculated according to the velocities of the elementary particles in the former time step k, as shown in Eq. (23).

$$\vec{L} = m \cdot \sum_i \left(\vec{r} k_i - \vec{r}_g^{\,k} \right) \times \vec{u}_i^{\,\prime\, k+1} \tag{23}$$

where, $\vec{L}$ is angular momentum, m is mass of CA particle, $\vec{u}'$ is velocity vector after revising the position of elementary particles, k is time step, $\vec{r}_g^{\,k}$ is center position of CA particle at time step k.

Based on the conservation of angular momentum, the angular velocity of each CA particle in the step k+1 is obtained.

$$\vec{I}_g^{\,k} \cdot \vec{\omega}^{k+1} = \vec{L} \tag{24}$$

$$\vec{\omega}^{k+1} = m \left(\vec{I}_g^{\,k} \right)^{-1} \cdot \sum_i \left(\vec{r} k_i - \vec{r}_g^{\,k} \right) \times \vec{u}_i^{\,\prime\, k+1} \tag{25}$$

where, $\vec{I}_g^{\,k}$ is inertia tensor.

Then, the position and velocity of elementary particle can be revised by Eqs. (26) and (27).

$$\vec{r}_i^{\,k+1} = \vec{r}_i^{\,k} + \left(\vec{r}_g^{\,k+1} - \vec{r}_g^{\,k} \right) + \vec{\omega}^{k+1} \times \left(\vec{r}_i^{\,k} - \vec{r}_g^{\,k} \right) \Delta t \tag{26}$$

$$\vec{u}_i^{\,k+1} = \vec{u}_i^{\,k} + \left(\vec{u}_g^{\,k+1} - \vec{u}_g^{\,k} \right) + \vec{\omega}^{k+1} \times \left(\vec{r}_i^{\,k} - \vec{r}_g^{\,k} \right) \tag{27}$$

where, Δt is time interval.

On the right side of Eqs. (26) and (27), the second term represents the translation of whole rigid body, and the third term represents the motion of elementary particle due to the rotation of rigid body.

4. Experimental program and numerical simulation

4.1. Concrete mixtures and rheological properties

Two series of high fluidity concrete were numerically analyzed in this study, which had different segregation resistance. The mix proportions are given in Table 2. Ordinary Portland cement with the Blaine fineness of 3500 cm^2/g and the density of 3150 kg/m^3 was used. JIS type II fly ash with the Blaine fineness of 4392 cm^2/g and the density of 2300 kg/m^3 was used. The fine aggregate sea sand had the particle size of 0–5 mm and the surface dry density of 2590 kg/m^3, and its water absorption capacity was 1.36% and fineness modulus was 2.9. CA was crashed stone with the size of 5–20 mm and its surface dry density was 2730 kg/m^3. Water absorption capacity of CA was 0.47% and its fineness modulus was 6.72. The PSD (particle size distribution) curves of the sand and the CA used are shown in Fig. 18. The maximum packing volume fraction φ_m of CA was 59.2%. Using Eqs. (20) and (22), the volume fraction (φ') of CA in the CA particle system was calculated as 42.4%.

The slump flow tests of No.1 and No.2 were performed, as shown in

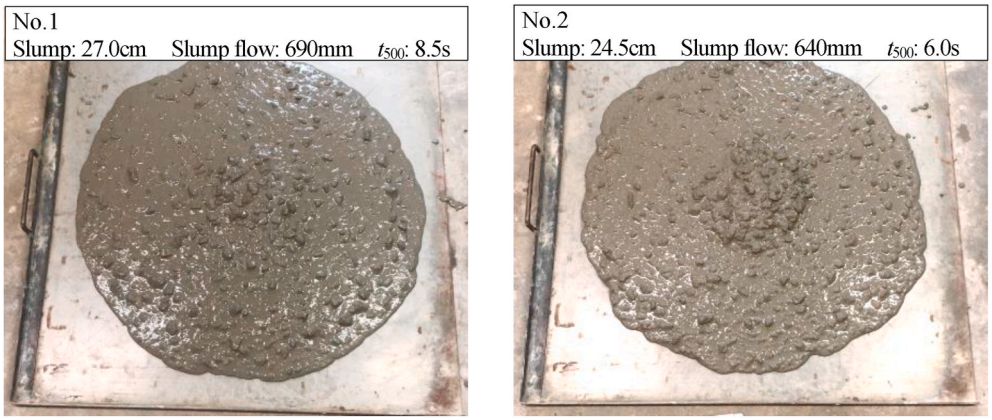

Fig. 19. Slump flow test and consistency of two high fluidity concretes.

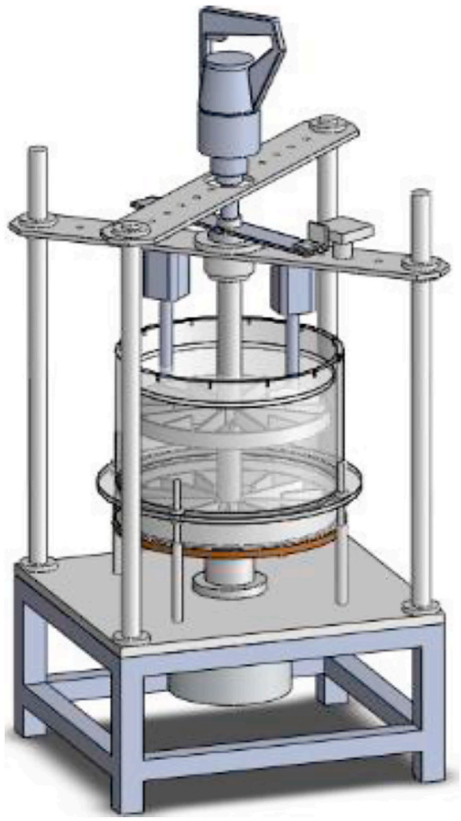

Fig. 20. RSNS rheometer.

Fig. 19, the test results are shown in Table 2. It was found that no segregation occurred in No.1, but the No.2 segregated, some CA particles were left in the center of the concrete sample. The Bingham constants of the matrix mortars and the fresh concretes were measured by the rheometer, called RSNS, as shown in Fig. 20, which is classified as parallel plate rheometer. The upper blade cannot rotate, but its subjected torque can be detected. During the measurement the torque should be over zero. The lower blade is driven by a motor. Using the rotation speed and torque of the lower blade, the shear strain rate and shear stress of the sample are calculated, further the plastic viscosity and yield stress are obtained [40]. Since the sedimentation of aggregate particles badly affects the measurement results of rheological parameters [41], after placing the fresh concrete samples into the RSNS rheometer, the measurement was performed as soon as possible. Based on the measured plastic viscosities and yield stresses of matrix mortars and fresh concretes, the values of intrinsic viscosity μ_* and intrinsic yield stress τ_* of two concretes were deduced to be 4.2 and 3.2, respectively, by using Eqs. (18) and (19). Finally, Eqs. (18) and (19) were used to calculate the Bingham constants of the CA particle system in the two series of concretes based on the Bingham constants of the matrix mortars. All the Bingham constants used in numerical simulation are shown in Table 3.

4.2. L-box flow test and segregation measurement

The L-box flow tests of two concretes were conducted and the segregation degrees of CA at different positions after flowing were evaluated. The test procedure was as follows:

(1) Right after mixing, fresh concrete sample was casted into the left vertical room of the L-box shown in Fig. 21.
(2) The gate was lifted up quickly within 1 s.
(3) After the concrete sample stopped flowing, the flow distance and flow time were recorded. Then, the concrete was divided into 7 parts in the horizontal direction at an interval of 100 mm, as shown in Fig. 21. The volume of concrete in each part was measured.
(4) The CA in each part was sieved out with a 5 mm opening sieve and washed off the adhering mortar, then the volume of CA in each part in the surface dry state was measured. The volume fraction of CA in each part was further calculated.
(5) The segregation degree (*SD*) of fresh concrete in each part was calculated by Eq. (28). The more the *SD* deviates from 1.0, the more severe the segregation. The segregation of fresh concrete not only changes the volumetric content of CA in different zones, but also changes the PSD (particle size distribution) of CA in different zones [42]. Not only in the experiment but also in the simulation, if the numbers of CA particles of different size ranges are counted, the change of PSD can be evaluated easily. But for simplifying the segregation analysis here, we only evaluated the variation of CA volume fraction in different zones.

$$SD_i = \varphi_i / \overline{\varphi} \tag{28}$$

where, SD_i is segregation degree of CA in part i, φ_i is volume fraction of CA in part i, $\overline{\varphi}$ is volume fraction of CA of whole concrete.

4.3. Configuration of numerical simulation

The L-box flow simulations were conducted for the two series of concrete using the I-MPS method and the DPMP model. As discussed in Section 2.4, for ensuring the simulation accuracy, the diameter of mortar particle and elementary particle was set to 5 mm. The number of coarse aggregate particles in Series No.1 and No.2 was 1754 (number of elementary particles: 6774) and 1982 (number of elementary particles: 7561), respectively, which randomly distributed in the matrix mortar.

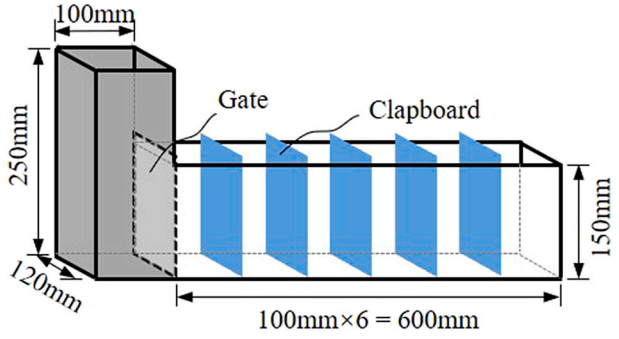

Fig. 21. Geometry of L-box.

Table 3
Rheological parameters of materials.

Series	No.1			No.2		
Parameter	Mortar	Concrete	Coarse aggregate (calculated)	Mortar	Concrete	Coarse aggregate (calculated)
Plastic viscosity (Pa·s)	79.7	508.6	1826.2	43.9	376.9	1005.9
Yield stress (Pa)	12.6	21.3	31.5	8.7	16.2	21.8

Table 4
Configuration information of particles.

Series of concrete	Double-phase & multi-particle model					
	Mortar particle			Coarse aggregate particle		
	Density	Shape, diameter	Number	Density	Shape, size distribution	Number
No.1	2.215	Sphere, 5 mm	15076	2.730	Random,	1754
No.2	2.230		14289		5–10 mm, 28% 10–15 mm, 36% 15–20 mm, 36%	1982

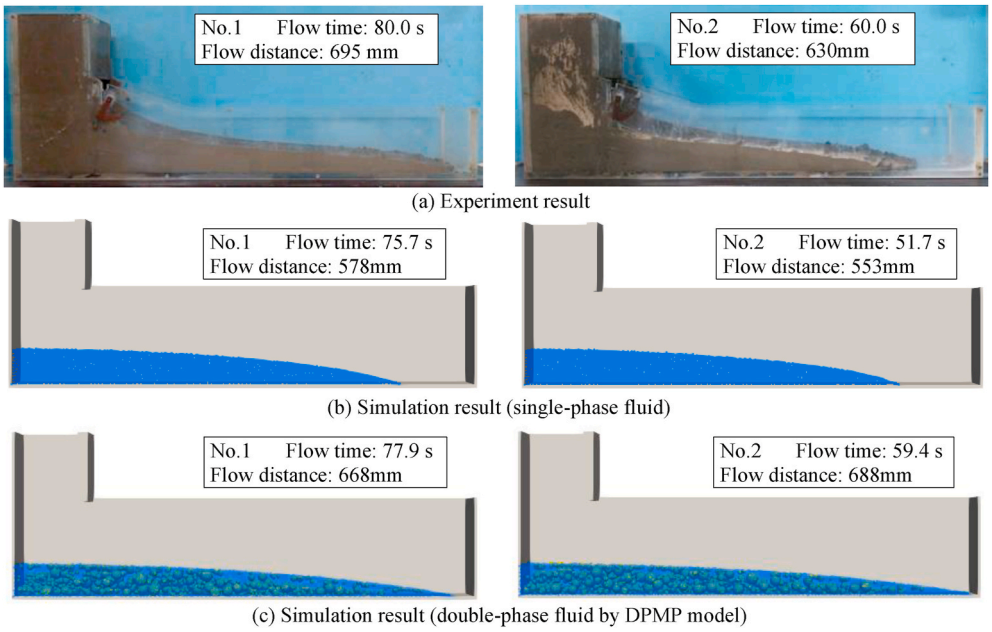

Fig. 22. Final flow shape of the fresh concrete in the L-box flow test.

The numbers of matrix mortar particles are shown in Table 4. The volume fractions of CA particles in the range of 5–10 mm, 10–15 mm and 15–20 mm were set to be 28%, 36%, and 36%, respectively, for making the fineness modulus (F.M.) of simulated coarse aggregate to be consistent with the experimental value (F.M. = 6.72). The detailed configuration information of particles was shown in Table 4.

5. Results and discussion

5.1. L-box flow behavior

After lifting the gate of L-box, the concrete sample quickly flowed out from the vertical room into the horizontal room. In the experiments, the flow time (t_{stop}) of No.1 was 80.0 s, and the flow distance was 695 mm, but the flow of No.2 stopped after 60.0 s, and the flow distance was 630 mm. The final shapes of the L-box flow are shown in Fig. 22(a). In numerical simulations, both two series of L-box flow were simulated twice, by using a single-phase fluid model and the DPMP model, respectively. The final flow shapes obtained by the simulations are shown in Fig. 22(b) and (c). In the experiment, the flow velocity of the concrete gradually decreased with the flowing time, and eventually became zero when the gravity-induced shear stress was less than the yield stress. However, in the numerical simulation, particle velocity became smaller and smaller, but it never reached zero due to the use of regularized Bingham model [43]. In this study, it was assumed that when the flow velocity was less than 1 mm/s, the flow of concrete was considered to stop. The criterion of flow stop is a common issue, which affects slightly the numerical result of flow distance and thus needs to be discussed in the future.

When using the single-phase fluid, the flow of No.1 and No.2 stopped at 75.7 s and 51.7 s, the flow distances were 578 mm and 553 mm, respectively. However, when using the DPMP model, the flow of No.1

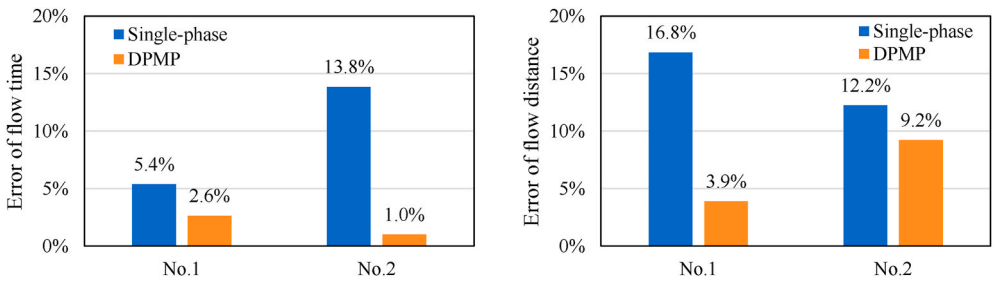

Fig. 23. Errors between the numerical and experimental results.

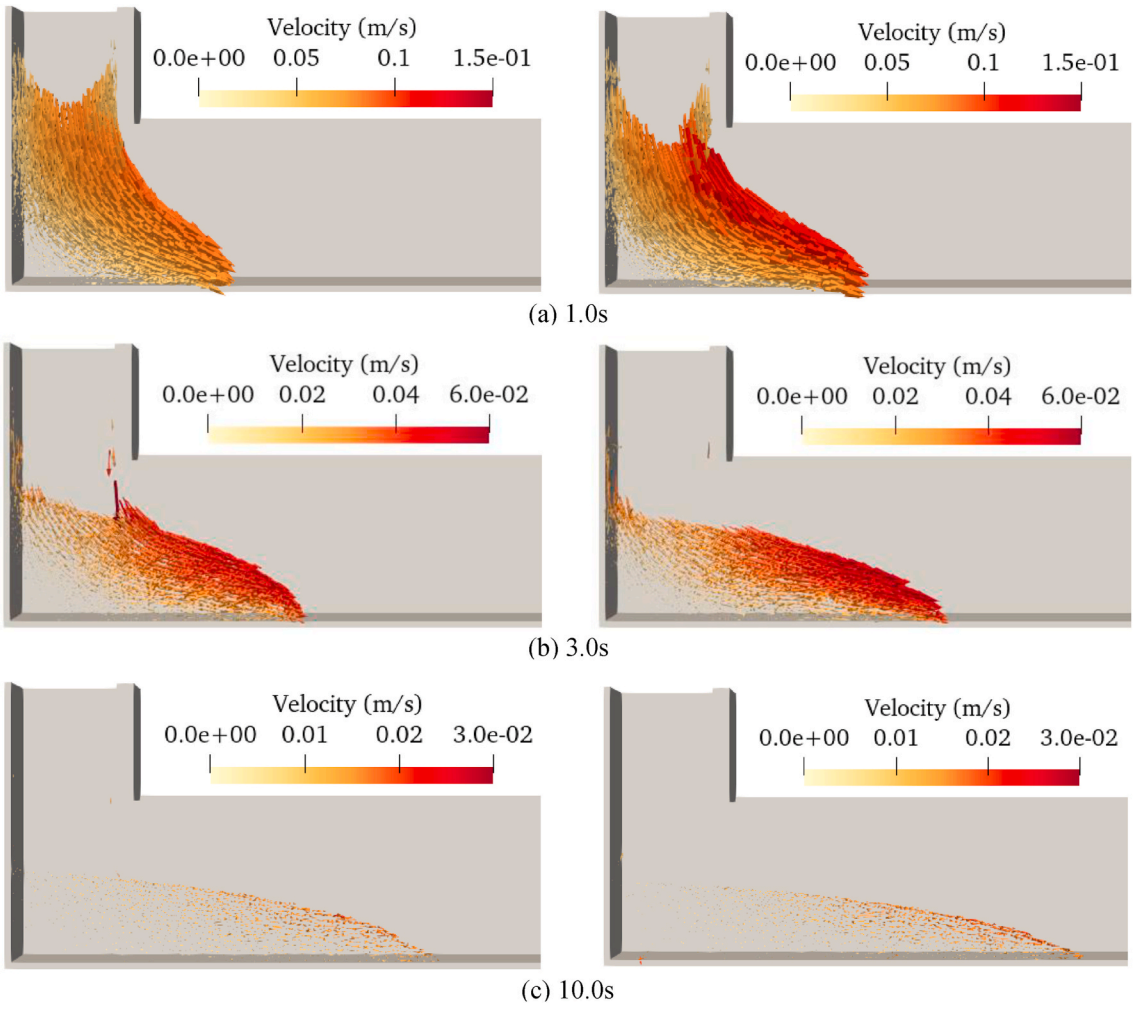

Fig. 24. Velocity profile of fresh concrete simulated by using DPMP model (Left: No.1, Right: No.2).

and No.2 stopped at 77.9 s and 59.4 s, and the flow distances were 668 mm and 688 mm, respectively. The errors between the numerical and experimental results were calculated by Eq. (29), as shown in Fig. 23. The errors of flow stop time and flow distance when using the DPMP model were less than 10%. Compared with the single-phase fluid model, the simulations using the DPMP model proposed in this study gave the flow stop times and flow distances that were closer to the experimental results. The plastic viscosity of No.2 was smaller than that of No.1. Therefore, the L-flow of No.2 was faster, and thus the numerical flow distance until the flow velocity gradually decreased to 1 mm/s was larger than the experimental result.

$$Error = \frac{|simulation\ result - experimental\ result|}{experimental\ result} \times 100\% \tag{29}$$

The flow behaviors of fresh concretes were simulated using the DPMP model, obtained velocity distributions are shown in Fig. 24. The velocity direction of the particle is indicated by arrow, and the length and color of the arrow represent the magnitude of the particle velocity. Since the flow of fresh concrete near the walls or bottom of L-box was affected by the boundary resistance, the flow velocities of the particles were low. The concrete sample at the left bottom corner was subjected to two boundary resistances from the side and the bottom of L-box at the same time, thus the concrete sample was hard to flow. However, the

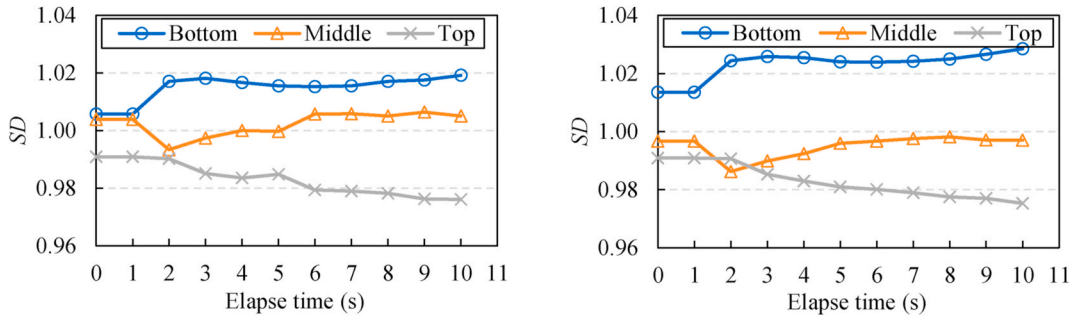

Fig. 25. Static segregation degree of CA in each part (left: No.1, right: No.2).

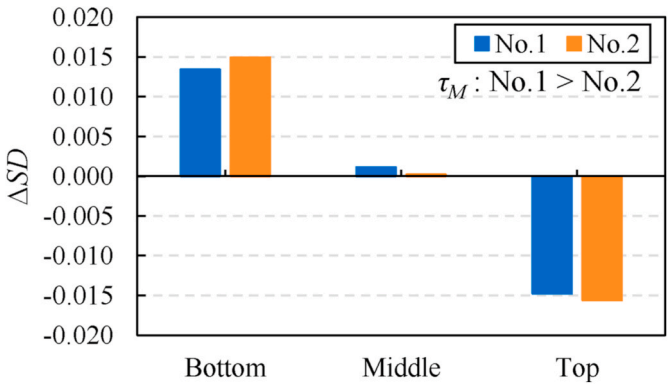

Fig. 26. Change of *SD* before and after static segregation.

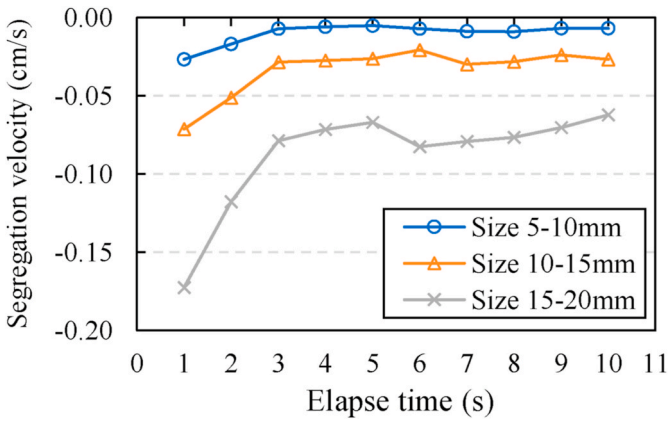

Fig. 27. Segregation velocities of CA particles with different size ranges (static segregation, No.2).

concretes near the free top surface and in the front of the flow flowed very quickly. After the concrete sample rushed out of the vertical room to enter into the horizontal room, the flow direction changed, and the flow velocity rapidly decreased, and the lower part of concrete eventually stopped, but the upper concrete in the flow front continued to flow forward slowly for a certain time. Since No.2 had lower plastic viscosity, it flowed faster than No.1.

5.2. Segregation simulation of fresh concrete

5.2.1. Static segregation

To simulate and analyze the static segregation of coarse aggregate, the concrete sample in the vertical room was allowed to stand for 10 s before the gate was lifted up. Although the static segregation degree within 10 s is not great, the qualitative analysis of static segregation is possible by the simulation of 10 s. The concrete in the vertical room of L-box was equally divided into three parts (bottom, middle, and top), and the *SD* of CA in each part was recorded over time, as shown in Fig. 25. Since the CA particles settled down in the fresh concrete, the *SD* of the top part was less than 1.0, and gradually decreased, while the *SD* in the bottom concrete was larger than 1.0, and approached to a certain value. However, the segregation of CA will not be so serious that CA reaches its maximum packing volume fraction [44].

Fig. 26 shows the changes of segregation degree (ΔSD) of different parts in concrete No.1 and No.2 in standing period. Since the matrix mortar in No. 2 had a lower yield stress, the ΔSD of No.2 was larger than that of No.1. It should be noted that since the regularized Bingham constitutive equation in Eq. (2) was used in this study, the effect of the yield stress of fresh concrete was slightly weakened (see Fig. 1), which may lead to a slightly large calculation of static segregation. Hence,

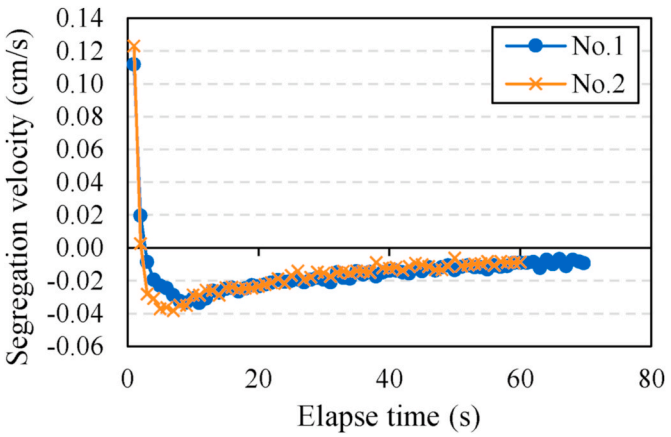

Fig. 28. Vertical segregation velocities of CA particles in different concrete (dynamic segregation).

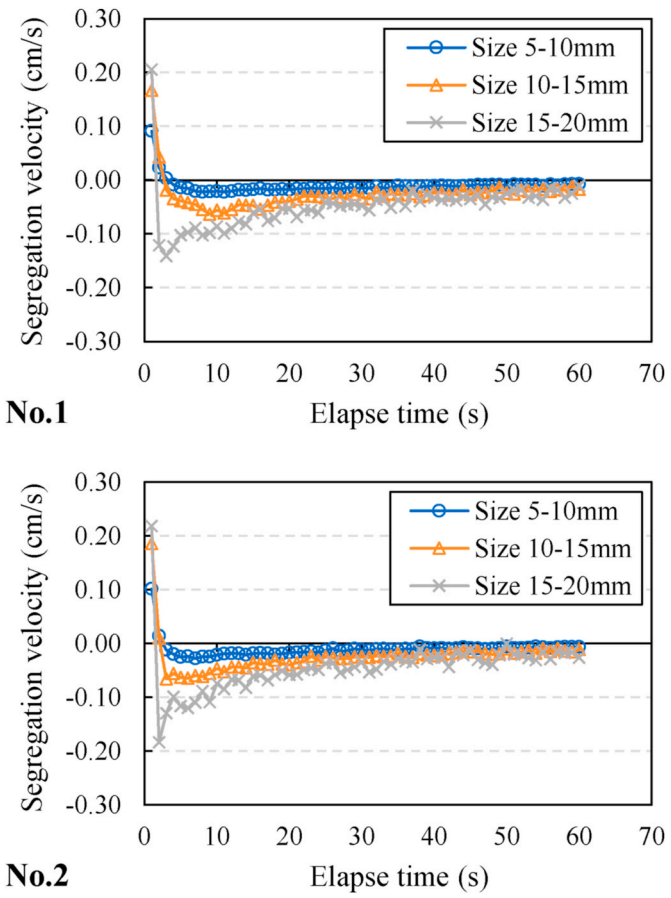

Fig. 29. Vertical segregation velocities of CA particles with different sizes (dynamic segregation).

slight segregation was also observed in the concrete No.1. Also, since the difference in density between coarse aggregate and mortar in No.1 and No.2 is almost the same, and the observation time was not long enough, the CA segregation degrees of the two concretes were close.

Here, we defined the difference of moving velocities between CA particle and surrounding mortar as the segregation velocity of the CA particle, and vertical upward and horizontal right are set to be positive directions. Fig. 27 shows the segregation velocity of CA particles with different size ranges in the vertical direction. The static segregation velocities of CA particles are fast at the beginning, and then approach to

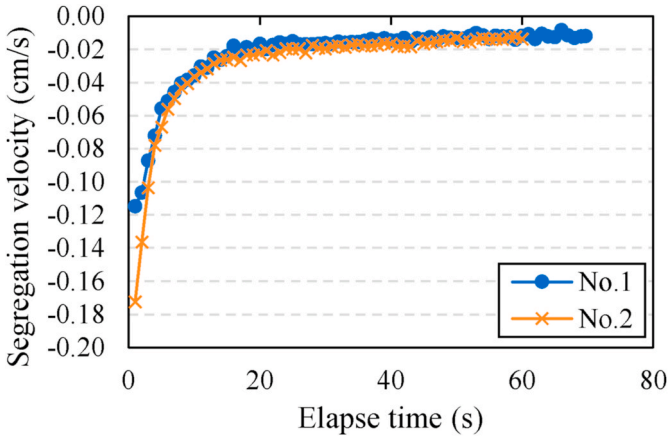

Fig. 30. Horizontal segregation velocities of CA particles in different concrete (dynamic segregation).

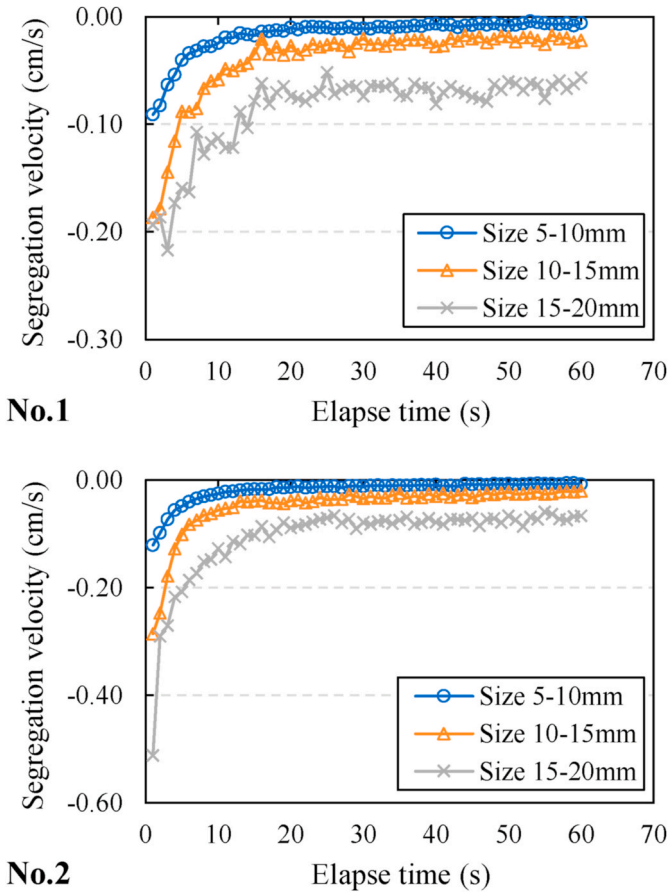

Fig. 31. Horizontal segregation velocities of CA particles with different sizes (dynamic segregation).

certain values, the smaller the CA particle, the smaller the static segregation velocity. The numerical results discussed above agree with the theoretical analysis by Roussel [44], which is that small particles do not easily segregate, the moving speed of larger particle is greater. Due to the segregation, the volume fraction of CA at the bottom of concrete sample increases, thereby enhancing the particle lattice effect (PLE) and the stability of the concrete [45].

5.2.2. Dynamic segregation

During the flow, the dynamic segregation of CA may occur not only in the vertical direction, but also in the horizontal direction. Right after the gate of L-box was opened, the fresh concretes flowed out rapidly, and the height of concrete in the vertical room decreased quickly. Because of greater gravity and standstill inertia of CA, its downward movement speed was less than that of the surrounding matrix mortar at the beginning. As the concrete flowed out of the vertical room, the flow speed of the concrete gradually decreased. However, the CA particles continued to move horizontally at a relatively large speed due to their greater motion inertia. Finally, with the stop of the concrete flow and the gradual increase of the CA volume fraction in the bottom concrete, the dynamic segregation velocity in the vertical direction gradually decreased. The vertical segregation velocities of CA particles in both concretes No.1 and No.2 are shown in Fig. 28. Within 10 s, the segregation velocity of No.2 was larger than that of No.1. Fig. 29 shows the dynamic segregation velocities of CA particles with different dimensions in the vertical direction. During flowing, the larger the CA particle, the greater the vertical segregation velocity of the CA particle.

In the horizontal direction, the flow velocity was the fastest immediately after the gate was opened, i.e., the deformation rate of the fluid was the largest. The CA particles stayed still due to their gravity and standstill inertia, but the matrix mortar had a higher flow velocity at the beginning of the concrete flow. The difference in flow velocity between matrix mortar and CA was large, which leads to a large shear-induced segregation velocity at the beginning [42]. The flow velocity of matrix mortar gradually decreased and the flow velocity of CA increased due to motion inertia, their flow velocity difference decreased, thus the segregation velocity decreased accordingly. Fig. 30 shows the horizontal segregation velocity of CA particles in No.1 and No.2. The CA segregation velocity of No.2 was larger than that of No.1. Fig. 31 shows the change of segregation velocity of CA particles in the horizontal direction with the dimensions of CA particles. The results show that the larger the CA particle, the greater the dynamic segregation velocity.

Small plastic viscosity of matrix mortar will cause it to have a little force to prevent the segregation of CA particles, which leads to poor dynamic stability of concrete [42,46]. The yield stress and plastic viscosity of the matrix mortar of No. 2 were smaller than those of No. 1, thus the matrix mortar of No.2 had a lower ability to prevent the segregation of CA particles in the initial flow stage. In addition, since the specific surface area of CA particle is proportional to the magnitude of the force resisting its segregation, the larger the CA particle, the smaller the force from matrix mortar resisting its segregation [46]. Therefore, the dynamic segregation velocity of No. 2 in the vertical direction was higher than that of No. 1, and the vertical segregation velocity of CA particles with the size of 15–20 mm was the largest. As the flow became slow, the shear rate decreased, and the shear-induced segregation slowed down.

After the concrete stopped flowing, the segregation degree of CA in each horizontal part was calculated according to Eq. (14). The experimental and numerical results are shown in Fig. 32. When fresh concrete flowed through the gate of L-box, the flow velocity direction changed dramatically in the horizontal distance of 10–40 cm, the coarse aggregate segregated due to the effect of standstill inertia. This explains why the segregation degree was larger in the horizontal range of 10–40 cm near the gate of L-box. Fig. 33 shows the position change of three parts of concrete No.1 in the vertical room during the flow in L-box. It was found that the concrete in the flow front mainly came from the top part of concrete in the vertical room. And from Fig. 25, it was found that the CA in the top part of concrete in the vertical room was the least. This can explain why the *SD* in the 50–70 cm range was small, as shown in Fig. 32. The difference between the numerical and the experimental results in this range was mainly due to the assumption that there was no slip between the concrete and the bottom of L-box in the simulation. Therefore, it is necessary to study the slip behavior of concrete on the boundary, which will be reported in detail in our other paper.

In addition, there are many other reasons for the inconsistency between the numerical and the experimental results, including initial

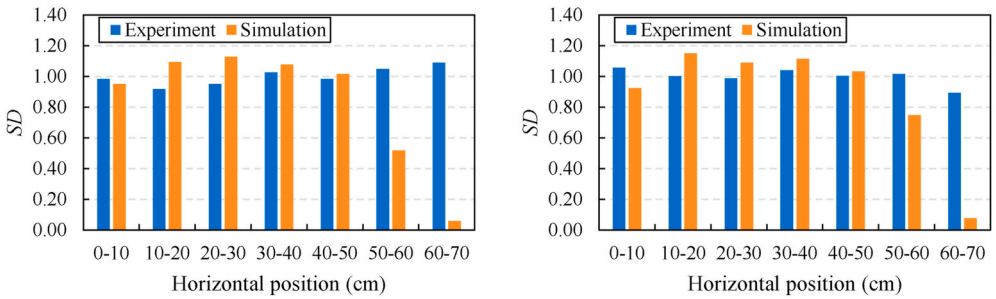

Fig. 32. Segregation degree of CA in different horizontal ranges (left: No.1, right: No.2).

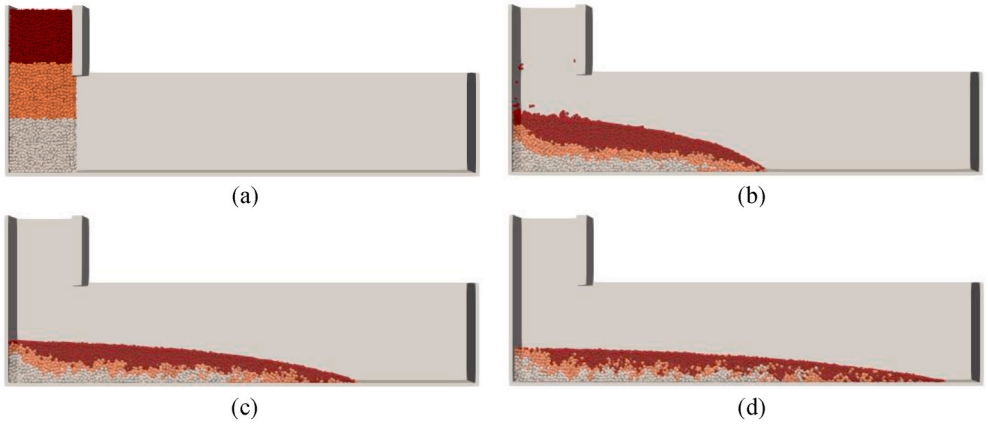

Fig. 33. Position change of three parts of fresh concrete in the vertical room during the L-flow (No.1).

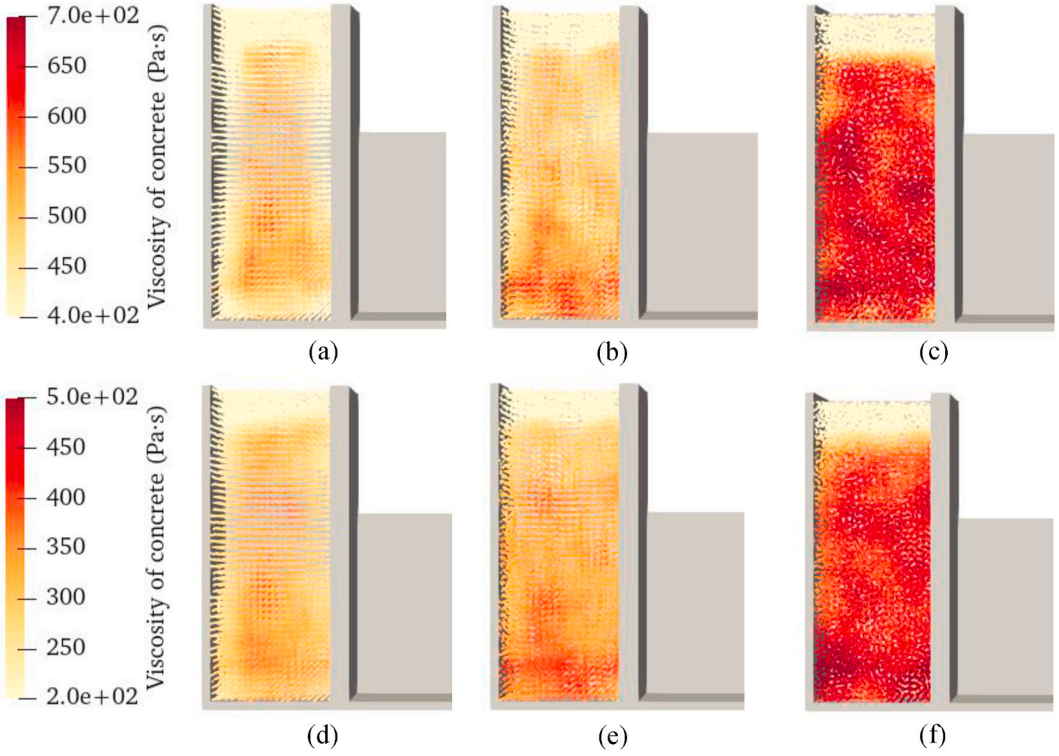

Fig. 34. Viscosity distribution of fresh concrete in the vertical room after static segregation (upper: No.1, lower: No.2).

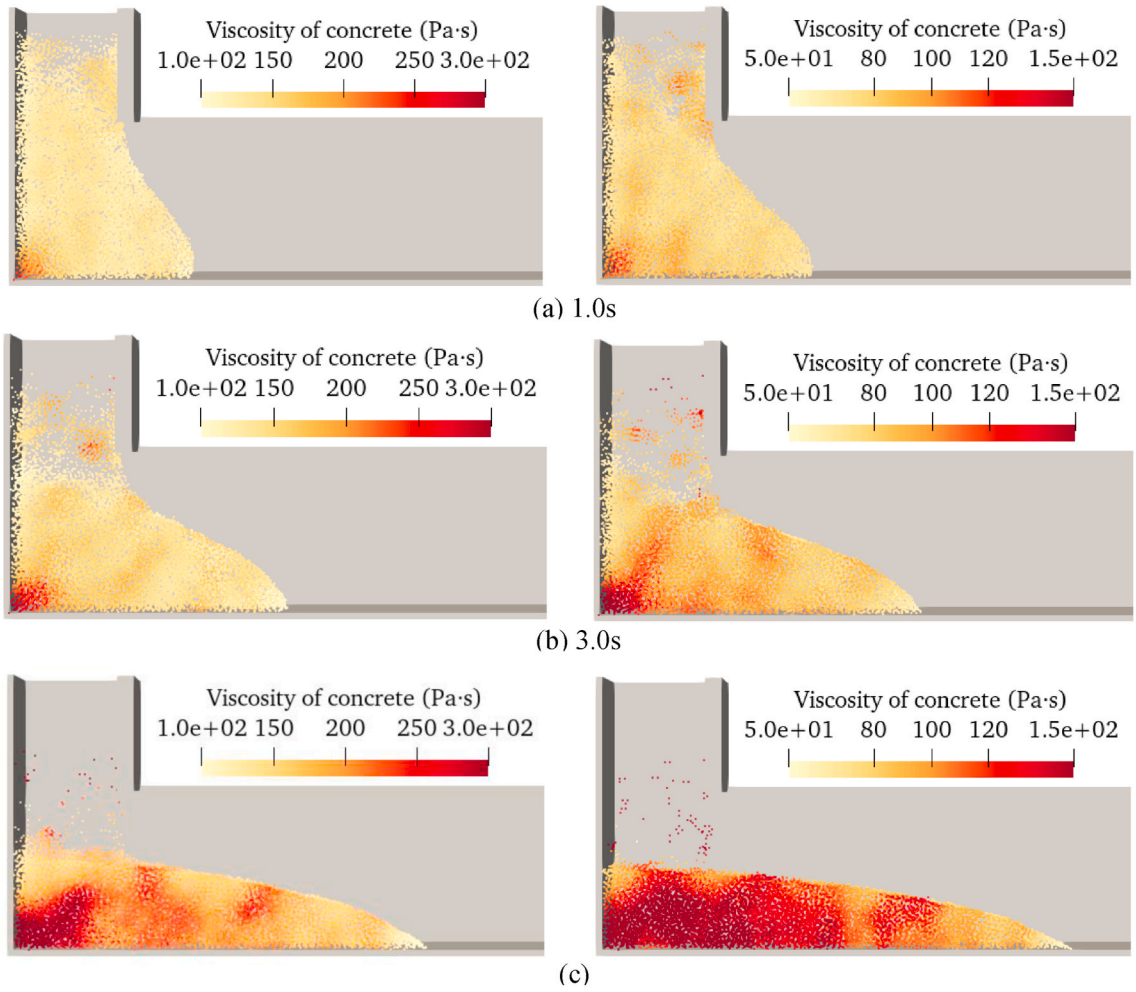

Fig. 35. Viscosity distribution of fresh concrete after dynamic segregation (Left: No.1, Right: No.2).

distribution of CA particles in the vertical room of L-box, the differences in the shapes and dimensions of CA particles from their actual situation, and the measurement accuracy of the Bingham constants of fresh concrete and fresh matrix mortar. Moreover, it is known that even for the same fresh concrete, different rheometers would give different measuring results of rheological parameters (yield stress and plastic viscosity) [47]. Therefore, it is difficult to match completely the numerical results with the experimental results. Nevertheless, this study aims to develop a numerical approach which has the ability to predict the segregation behavior of fresh concrete. Although part of the simulation results was not fully consistent with the experimental results, the proposed numerical approach still has potential to simulate both the static and dynamic segregation behaviors of fresh concrete, and show the uneven distribution of CA particles in fresh concrete.

5.3. Dynamic viscosity distribution

Based on Eq. (17), the dynamic viscosity distribution at different flow times were calculated. Fig. 34 shows the calculating results for different flow times (1.0s, 3.0s, and 10.0s) after the static segregation in the vertical room of L-box before opening the gate. With the static segregation, i.e., as part of CA particles settle down, the viscosity of the concrete at the lower position gradually increases.

The uneven distribution of dynamic viscosity, induced by the dynamic segregation occurring during the flow can also be clarified, as shown in Fig. 35. As explained in Section 5.1, due to the two boundary resistances the concretes have a high dynamic viscosity at the left-bottom corner. Along the flow direction, dynamic viscosity decreases, and in the rear of the flow, the dynamic viscosity of the concrete gradually increases with flow time, but the concrete in the front of flow has low dynamic viscosity because of less CA and more mortar. Also, it can be found that No.1 has a lower unevenness of dynamic viscosity than No.2. This is because that No.1 has greater Bingham constants than No.2.

6. Conclusions

In this study, a double-phase & multi-particle (DPMP) model was developed and used in the flow simulation of fresh concrete. Based on this constitute model of fresh concrete and the I-MPS method, a numerical flow approach was proposed to simulate the flow behavior and the segregation behavior of fresh concrete. This numerical flow approach was verified by the L-flow simulation of two high fluidity concretes. The following conclusions can be drawn:

(1) The proposed numerical flow approach of fresh concrete can well simulate the flow behavior of fresh concrete, which is regarded as a double-phase fluid composed of matrix mortar and coarse aggregate (CA) with a particle size distribution and random particle shapes. The proposed numerical flow approach has higher accuracy than normal simulation treating fresh concrete as a homogeneous fluid.
(2) For the use of the DPMP model, the interactions between mortar-mortar particles, CA-CA particles, mortar-CA particles were

quantitatively discussed, respectively. The densities of matrix mortar and coarse aggregate were also differentiated according to their actual values. The proposed numerical flow approach can predict the movement of coarse aggregate and simulate the segregation behavior of CA particles from matrix mortar. Moreover, the numerical flow approach can also clarify the change in the viscosity of fresh concrete after the segregation of coarse aggregate.

(3) The CA segregation can be divided into static segregation and dynamic segregation. The segregation of CA particle is associate with its size and the rheological parameters of matrix mortar. The larger the CA particle, the easier its segregation, and the larger the segregation velocity. The smaller the yield stress of matrix mortar, the easier it is for CA to segregate. The greater the plastic viscosity of matrix mortar, the lower the segregation velocity. The inertial force of CA and the flow rate of fresh concrete also influence the dynamic segregation of CA. The greater the gravity (i.e., the inertial force due to gravity) of CA particle or the higher the flow speed of fresh concrete, the more likely the CA particles will segregate.

Declaration of competing interest

The authors declare that they have no known competing financial interests or personal relationships that could have appeared to influence the work reported in this paper.

References

[1] H. Okamura, M. Ouchi, Self-compacting concrete, J. Adv. Concr. Technol. 1 (2003) 5–15.
[2] Z. Li, State of workability design technology for fresh concrete in Japan, Cement Concr. Res. 37 (2007) 1308–1320.
[3] L. Shen, L. Struble, D. Lange, Testing static segregation of SCC, in: SCC2005, Proc. 2nd North Am. Conf. Des. Use SCC, 2005, pp. 1–3.
[4] D.K. Panesar, B. Shindman, The effect of segregation on transport and durability properties of self consolidating concrete, Cement Concr. Res. 42 (2012) 252–264.
[5] J. Pan, X. Gao, H. Ye, Influence of rheological behavior of mortar matrix on fresh concrete segregation and bleeding, Iran, J. Sci. Technol. - Trans. Civ. Eng. (2020) 1–15.
[6] L. Shen, H. Bahrami Jovein, Z. Sun, Q. Wang, W. Li, Testing dynamic segregation of self-consolidating concrete, Construct. Build. Mater. 75 (2015) 465–471.
[7] P. Turgut, K. Turk, H. Bakirci, Segregation control of SCC with a modified L-box apparatus, Mag. Concr. Res. 64 (2012) 707–716.
[8] J. Han, K. Wang, X. Wang, P.J.M. Monteiro, 2D image analysis method for evaluating coarse aggregate characteristic and distribution in concrete, Construct. Build. Mater. 127 (2016) 30–42.
[9] M.I. Safawi, I. Iwaki, T. Miura, The segregation tendency in the vibration of high fluidity concrete, Cement Concr. Res. 34 (2004) 219–226.
[10] X. Gao, J. Zhang, Y. Su, Influence of vibration-induced segregation on mechanical property and chloride ion permeability of concrete with variable rheological performance, Construct. Build. Mater. 194 (2019) 32–41.
[11] J. Spangenberg, N. Roussel, J.H. Hattel, H. Stang, J. Skocek, M.R. Geiker, Flow induced particle migration in fresh concrete: theoretical frame, numerical simulations and experimental results on model fluids, Cement Concr. Res. 42 (2012) 633–641.
[12] S. Hurukawa, Y. Kato, M. Suzuki, S. Takahashi, Effect of mortar viscosity and coarse aggregate amount on segregation of high-fluidity concrete, Proc. Japan Concr. Inst. 42 (2020) 989–994 (in Japanese).
[13] G.R. Liu, M.B. Liu, Smoothed Particle Hydrodynamics, World Scientific Publishing Co. Pte Ltd, 2003.
[14] Z. Xu, Z. Li, F. Jiang, The applicability of SPH and MPS methods to numerical flow simulation of fresh cementitious materials, Construct. Build. Mater. 274 (2021) 121736.
[15] G. Cao, Z. Li, Z. Xu, A SPH simulation method for opening flow of fresh concrete considering boundary restraint, Construct. Build. Mater. 198 (2019) 379–389.
[16] W.S. Alyhya, S. Kulasegaram, B.L. Karihaloo, Simulation of the flow of self-compacting concrete in the V-funnel by SPH, Cement Concr. Res. 100 (2017) 47–59.
[17] S. Urano, H. Nemoto, K. Sakihara, Application of flow simulation for evaluation of filling-ability of self-compacting concrete, J. Japan Soc. Civ. Eng. Ser. E2 (Materials Concr. Struct. 68 (2012) 38–48 (in Japanese).
[18] H. Zhu, N.S. Martys, C. Ferraris, D. De Kee, A numerical study of the flow of Bingham-like fluids in two-dimensional vane and cylinder rheometers using a Smoothed Particle Hydrodynamics (SPH) based method, J. Nonnewton. Fluid Mech. 165 (2010) 362–375.
[19] T.C. Papanastasiou, Flows of materials with yield, J. Rheol. 31 (1987) 385–404.
[20] F. Galbusera, F. Niemeyer, Chapter 14 - mathematical and finite element modeling, in: F. Galbusera, H.-J. Wilke (Eds.), Biomech. Spine, Academic Press, 2018, pp. 239–255.
[21] A. Khayyer, H. Gotoh, A 3D higher order Laplacian model for enhancement and stabilization of pressure calculation in 3D MPS-based simulations, Appl. Ocean Res. 37 (2012) 120–126.
[22] S. Kulasegaram, B.L. Karihaloo, A. Ghanbari, Modelling the flow of self-compacting concrete, Int. J. Numer. Anal. Methods GeoMech. 35 (2011) 713–723.
[23] C.T. Kennedy, The design of concrete mixes, ACI J. Proc. 36 (1940) 373–400.
[24] T.C. Powers, The Properties of Fresh Concrete, Wiley, 1968.
[25] A. Shakibaeinia, Y.C. Jin, MPS mesh-free particle method for multiphase flows, Comput. Methods Appl. Mech. Eng. 229–232 (2012) 13–26.
[26] G. Duan, B. Chen, S. Koshizuka, H. Xiang, Stable multiphase moving particle semi-implicit method for incompressible interfacial flow, Comput. Methods Appl. Mech. Eng. 318 (2017) 636–666.
[27] C.F. Ferraris, F. De Larrard, N. Martys, Fresh concrete rheology - recent developments, Mater. Sci. Concr. VI. 6 (2001) 215–241.
[28] C.F. Ferraris', F. de Larrard, Testing and Modelling of Fresh Concrete Rheology, 1998. Gaithersburg, MD.
[29] A. Einstein, A new determination of molecular dimensions, Ann. Phys. 19 (1906) 289–306.
[30] R. Roscoe, The viscosity of suspensions of rigid spheres, Br. J. Appl. Phys. 3 (1952) 267–269.
[31] I.M. Krieger, T.J. Dougherty, A mechanism for non-Newtonian flow in suspensions of rigid spheres, Trans. Soc. Rheol. 3 (1959) 137–152.
[32] L.J. Struble, G.-K. Sun, Cement viscosity as A function of concentration, MRS Proc 289 (1992) 173.
[33] X. Chateau, G. Ovarlez, K.L. Trung, Homogenization approach to the behavior of suspensions of noncolloidal particles in yield stress fluids, J. Rheol. 52 (2008) 489–506.
[34] A. Ghanbari, B.L. Karihaloo, Prediction of the plastic viscosity of self-compacting steel fiber reinforced concrete, Cement Concr. Res. 39 (2009) 1209–1216.
[35] J. Yammine, M. Chaouche, M. Guerinet, M. Moranville, N. Roussel, From ordinary rheology concrete to self compacting concrete: a transition between frictional and hydrodynamic interactions, Cement Concr. Res. 38 (2008) 890–896.
[36] F. Mahaut, S. Mokéddem, X. Chateau, N. Roussel, G. Ovarlez, Effect of coarse particle volume fraction on the yield stress and thixotropy of cementitious materials, Cement Concr. Res. 38 (2008) 1276–1285.
[37] A. Salinas, D. Feys, Estimation of lubrication layer thickness and composition through reverse engineering of interface rheometry tests, Materials 13 (2020) 1799.
[38] N.S. Klein, S. Cavalaro, A. Aguado, I. Segura, B. Toralles, The wetting water in cement-based materials: modeling and experimental validation, Construct. Build. Mater. 121 (2016) 34–43.
[39] S. Koshizuka, A. Nobe, Y. Oka, Numerical analysis of breaking waves using the moving particle semi-implicit method, Int. J. Numer. Methods Fluid. 26 (1998) 751–769.
[40] Z. Li, Rheological model and rheometer of fresh concrete, J. Struct. Constr. Eng. (Transactions AIJ). 80 (2015) 527–537 (in Japanese).
[41] D. Feys, K.H. Khayat, Particle migration during concrete rheometry: how bad is it? Mater. Struct. Constr. 50 (2017).
[42] B.I.O. Koura, M. Hosseinpoor, A. Yahia, Coupled effect of fine mortar and granular skeleton characteristics on dynamic stability of self-consolidating concrete as a diphasic material, Construct. Build. Mater. 263 (2020) 120131.
[43] H. Lashkarbolouk, M.R. Chamani, A.M. Halabian, A.R. Pishehvar, Viscosity evaluation of SCC based on flow simulation in the L-box test, Mag. Concr. Res. 65 (2013) 365–376.
[44] N. Roussel, A theoretical frame to study stability of fresh concrete, Mater. Struct. Constr. 39 (2006) 81–91.
[45] B. Esmaeilkhanian, P. Diederich, K.H. Khayat, A. Yahia, H. Wallevik, Influence of particle lattice effect on stability of suspensions: application to self-consolidating concrete, Mater. Struct. Constr. 50 (2017).
[46] B. Esmaeilkhanian, K.H. Khayat, A. Yahia, D. Feys, Effects of mix design parameters and rheological properties on dynamic stability of self-consolidating concrete, Cement Concr. Compos. 54 (2014) 21–28.
[47] C.F. Ferraris, L.E. Brower, Comparison of concrete rheometers, Concr. Int.. 25 (2003) 41–47.